sustainability

MDPI

Article

The Influence of Selected Material Variables of Photocatalytic Cementitious Composites on the Self-Cleaning Properties and Air Purification Efficiency from NO_x Pollutants

Maciej Kalinowski *, Karol Chilmon, Wioletta Jackiewicz-Rek and Błażej Rakowski

Faculty of Civil Engineering, Warsaw University of Technology, 00-637 Warsaw, Poland
* Correspondence: maciej.kalinowski@pw.edu.pl

Abstract: This work aimed to investigate the influence of selected material variables on the self-cleaning and air purification efficiency in NO_x pollutants of cement-based photocatalytic composites. Tests were performed on cement mortars, with seven independent variables considered: the mass ratio between cement and quartz powder to sand, the water to cement ratio, the total mass amount of photocatalysts (two different types), the mass content of nanoparticulate silica, the percentage of quartz powder replacing part of cement, and the ratio between two sands of fine granulation. Photocatalytic cementitious materials had their self-cleaning properties tested via two methods (spectrophotometry—the degradation of rhodamine B under UVA irradiation, and the change in the contact angle—via a goniometer). Air purification properties were tested in the reaction chamber under UVA and visible light at low irradiance (0.2 W/m^2 for UVA, 150 W/m^2 for visible). It was found that TiO_2 content and the mass ratio between cement and quartz powder to sand were the most influential variables within the selected ranges of variability, with the ratio between sands and quartz content being the least significant variable of the tested properties.

Keywords: cementitious composites; photocatalyst; nitrogen oxide; self-cleaning; spectrophotometry; goniometer; air purification

Citation: Kalinowski, M.; Chilmon, K.; Jackiewicz-Rek, W.; Rakowski, B. The Influence of Selected Material Variables of Photocatalytic Cementitious Composites on the Self-Cleaning Properties and Air Purification Efficiency from NO_x Pollutants. *Sustainability* **2023**, *15*, 853. https://doi.org/10.3390/su15010853

Academic Editor: Qiao Ma

Received: 25 November 2022
Revised: 19 December 2022
Accepted: 26 December 2022
Published: 3 January 2023

1. Introduction

Environmental pollution caused by human activity has been a primary concern for flora, fauna, and human health, especially in urban areas [1]. The increase in the concentration of nitrogen oxides, ozone, and other elements requires the development of technology and techniques to reduce the influence on the environment. The use of cementitious photocatalytic composites provides a passive solution to the issue [2,3]. It contributes to air purification by lowering harmful NO_X and SO_X concentrations through photocatalytic reactions powered by sun radiation. According to the IUPAC (International Union of Pure and Applied Chemistry) definition, photocatalysis is a catalytic reaction based on light absorption by a photocatalyst [4]. The basic process in heterogeneous photocatalysis is the activation of a semiconductor, i.e., a photocatalyst, by irradiation. Semiconductors contain a band gap with energy E_g that separates the valence band from the conduction band. The photocatalysis process begins with energy absorption equal to or greater than E_g. Then, an h^+ hole is formed due to the transition of the e^- electron from the valence band to the conduction band. The resulting hole is a strong oxidant, while the electron is a reducing agent [5].

Acid rain and photochemical smog are severe problems for large urban agglomerations, as they can threaten human health and negatively affect plant metabolism [6]. Photocatalysts break down harmful chemicals such as nitrogen oxides. The process begins with the absorption of a quantum of solar radiation, which determines the formation of O_2 peroxide, which forms OH hydroxyl groups in contact with water [7]. Thanks to this,

oxidation reactions of harmful compounds take place. In cementitious materials, the resulting nitrate anions NO_3^- then react with the calcium to form a water-soluble salt—calcium nitrate—which is washed away by precipitation [8].

The most popular photocatalyst used in the photocatalytic cementitious materials discussed in this paper is titanium (IV) oxide. The first application of "titanium white" was as a dye, due to its strong brightening properties. However, the destructive effect of this additive on some organic dyes was noticed. At the end of the 1920s, this anomaly began to be studied, and theories related to the photocatalytic process were created [9]. Many semiconductors, e.g., ZnO, SnO_2, and ZnS, are tested for suitability in the photocatalytic process. However, titanium (IV) oxide is the most frequently described because of its high stability, availability, and non-toxicity [1]. It is obtained primarily from naturally occurring anatase (TiO_2), rutile (TiO_2), and ilmenite ($FeTiO_3$).

In a photocatalytic reaction, a photocatalyst (semiconductor such as titanium dioxide) is irradiated. Due to energy introduction, electrons (e^-) from the semiconductor shift from the valence band (vb) to the conduction band (cb), leading to the formation of electron holes h+ (Equation (1)). The resulting pairs of charges initiate a reduction–oxidation process (Figure 1). As this reaction mainly occurs in the air environment, in the presence of adsorbed oxygen and water (strong oxidants), it is possible to decompose a wide range of air pollutants due to the formation of hydroxyl radicals ($OH^{\cdot}$) and superoxide radicals ($O_2^{\cdot -}$) (Equations (2) and (3)) [5].

$$TiO_2 \overset{h\nu}{\rightarrow} TiO_2 + h_{vb}^+ + e_{cb}^- \quad (1)$$

$$(H_2O)_{ads} + h^+ \rightarrow H^+ + OH^{\bullet} \quad (2)$$

$$(O_2)_{ads} + e^- \rightarrow O_2^{\bullet -} \quad (3)$$

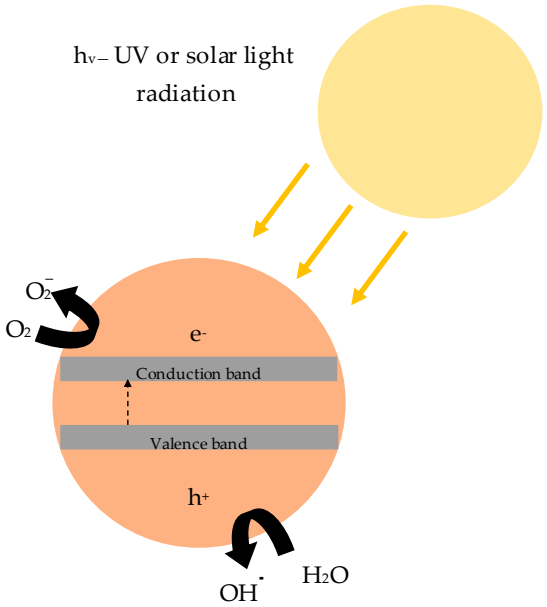

Figure 1. General mechanism of photocatalytic reaction.

Cementitious composites can be characterized by various properties, depending on the components used for their production [10,11]. Using photocatalysts in cementitious materials presents a new approach to improving air quality in urban areas. Most surfaces in cities are made with different cementitious materials (mainly concretes and mortars), and most pollutants are produced in their direct proximity due to human activity [12]. The placement of a passive system purifying the surrounding air built into those surfaces presents a solution worth considering. Photocatalytic mortars, or more widely, photocatalytic cementitious materials, represent a group of building materials that contribute to

improving air quality in urban areas. Sustainability can be understood in several ways, one of them being the counteraction to the negative influence of human activity on the environment. The composites in question have two functions—to act as a construction material (for roads, pavements, etc.) and, while doing so, to passively purify the air from harmful pollutants. Any research that covers methods or materials that contribute to a lesser impact of human activity on the surroundings could and should be considered a part of sustainable development.

The efficiency of photocatalytic reactions in cementitious materials depends on several variables, which can be divided into internal and external [13]. Toxic oxides are present in the air surrounding photocatalytic material, so parameters describing air's properties significantly impact the efficiency of photocatalytic reaction (mainly temperature, humidity, and air velocity). The internal factors, namely the properties of any given photocatalytic material—its chemical composition and morphology—and the interaction between titanium dioxide and other components of cementitious material also influence the intensity of the considered reactions [14].

In this paper, the authors decided to investigate the influence of the composition of a cementitious photocatalytic mortar on the intensity of photocatalytic reactions. As is well known, mortars consist of several different components—water, binder, and aggregate. In regular cementitious materials, changing the mass ratios between them results in a change in both mechanical properties and the overall durability of the material [15,16]. Titanium dioxide interacts with other components of the mix upon its addition to the material [17]. It has been observed that due to its grain size, when added in high concentrations, TiO_2 has an influence on the compressive strength of the hardened material [18]. It has also been observed that the efficiency of purifying the air from the aforementioned pollutants differs significantly in the case of TiO_2 powder and cementitious materials containing it—titanium oxide both agglomerates in the cement matrix and acts as nuclei for the products of cement hydration, reducing its exposure to sun radiation, and in consequence, on the surface of which photocatalytic reaction can occur [19]. Therefore, the composition of any cementitious mortar considered to be a TiO_2 carrier has an impact on its properties regarding photocatalytic reactions.

In the performed experiments, the influence of seven material variables on the mechanical and photocatalytic properties of cementitious mortars was investigated. The Plackett-Burman method (a screening design of an experiment, where an influence of several variables can be determined using a limited number of experiments; in the conducted study, the impact of seven variables was investigated with just 11 series of samples) was used, and the seven variables were defined –TiO_2 total mass, the mass ratio between two different photocatalysts (VLA, Visible Light Active and UV-A only, UV Light Active), the mass ratio between binder to aggregate, the mass ratio between water to cement, nanoparticulate silica mass content, replacement of cement with quartz powder, and the mass ratio between two aggregates of different granulation. In total, 11 cementitious mortar series were prepared and tested for consistency, mechanical properties including tensile and compressive strength, efficiency in purifying the air from NO_x pollutants, and efficiency in self-cleaning measured via two different tests (degradation of rhodamine under UVA radiation and the reduction in contact angle after exposure to UVA radiation).

2. Materials and Methods

A Plackett-Burman experimental design was prepared to investigate the influence of several material variables on selected properties of cementitious mortars. It is a screening design used to efficiently screen the impact of numerous variables on the chosen properties of any material. The prepared design considered seven variables on three levels (low, high, and average) and is presented in Table 1. A mass ratio of binder (cement and quartz powder—b) to sand (s) aggregate was considered in the range of 0.5 to 0.8 (b/s ratio in Table 1). A water-to-cement ratio was adopted from 0.35 to 0.43 (w/c ratio in Table 1). Nanoparticulate silica content was designed in a range from 10 to 40 kg/m^3. Quartz

powder content was described as a mass percentage of cement being replaced within the range of 5 to 15%. The influence of aggregate granulation was also included via the mass ratio between two aggregates of different granulation—0.5/1.2 and 0.1/0.5—within the range of 0.25 and 1. The influence of TiO_2 on selected properties was included via two last variables, the total mass content of titanium dioxide in the composite (5–20 kg/m^3) and the mass proportion between two types of photocatalyst being used in this study—TiO_2 (A) and TiO_2 (B)—within the range of 0.25 to 1.

Table 1. Values of designed independent variables in the experimental design.

Series ID											
Variable	**Unit**	**Range of Variability**	**1**	**2**	**3**	**4**	**5**	**6**	**7**	**8**	**9–11**
(b/s)	[-]	0.50–0.80	0.80	0.80	0.80	0.80	0.50	0.50	0.50	0.50	0.65
(w/c)	[-]	0.35–0.43	0.43	0.43	0.35	0.35	0.43	0.43	0.35	0.35	0.39
TiO_2 (A)/TiO_2 (B)	[-]	0.25–1.00	1.00	0.25	1.00	0.25	1.00	0.25	1.00	0.25	0.625
Nanoparticulatesilica	[kg/m^3]	10–40	40	40	10	10	10	10	40	40	25
Quartz powder	[%]	5–15	15	5	15	5	5	15	5	15	10
TiO_2	[kg/m^3]	5–20	20	5	5	20	20	5	5	20	12.5
Sand 0.5–1.2/0.1–0.5	[-]	0.25–1.00	1.00	0.25	0.25	1.00	0.25	1.00	1.00	0.25	0.625

2.1. Materials

The cement used in this study, CEM II/A-S 52.5R (Ożarów, Poland), met the requirements of EN 197-1 [20]. Its specific surface area was measured via the BET method and was 2.59 m^2/g, with its adsorption isotherm as specified in Figure 2.

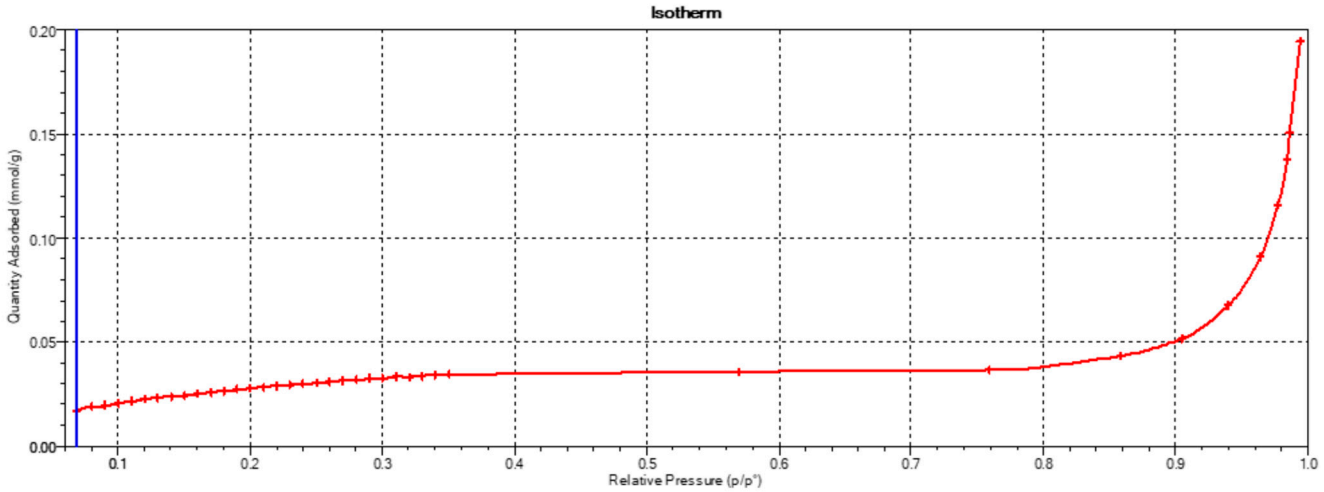

Figure 2. Adsorption isotherm of the CEM II A-S 52.5R.

The chemical composition of cement was investigated via the XRF method. The samples were dried to dryness at 105 °C. Then, they were poured into previously assembled special measuring cups. Samples prepared this way were placed in the XRF apparatus and measured. Losses on ignition (LOI) were determined. Material samples were dried to a constant weight and then subjected to the calcination process at 975 °C for 15 min. After cooling to room temperature, the samples were weighed. The percentage loss of the initial mass was the loss of ignition, which was included in the chemical composition results and is presented in Table 2.

Table 2. Summary of the results of the XRF analysis of cement (%), LOI—loss on ignition.

MgO	**Al_2O_3**	**SiO_2**	**P_2O_5**	**SO_3**	**Cl**	**K_2O**	**CaO**	**TiO_2**	**MnO**	**Fe_2O_3**	**CuO**	**ZnO**	**SrO**	**LOI**
1.883	3.227	18.989	0.257	3.765	0.042	0.894	65.336	0.277	0.078	2.832	0.019	0.032	0.067	0.011

The phase composition of cement was investigated via the XRD method. Cement samples, as in the case of XRF analysis, were dried. Then, they were placed in special steel holders and properly smoothed (a prerequisite for proper XRD measurement). The sample prepared in this way was placed in the measuring magazine and then in the diffractometer. The measurement was carried out in the range of 5–65° 2θ, with a single step of 0.02° 2θ lasting 5 s (Figure 3).

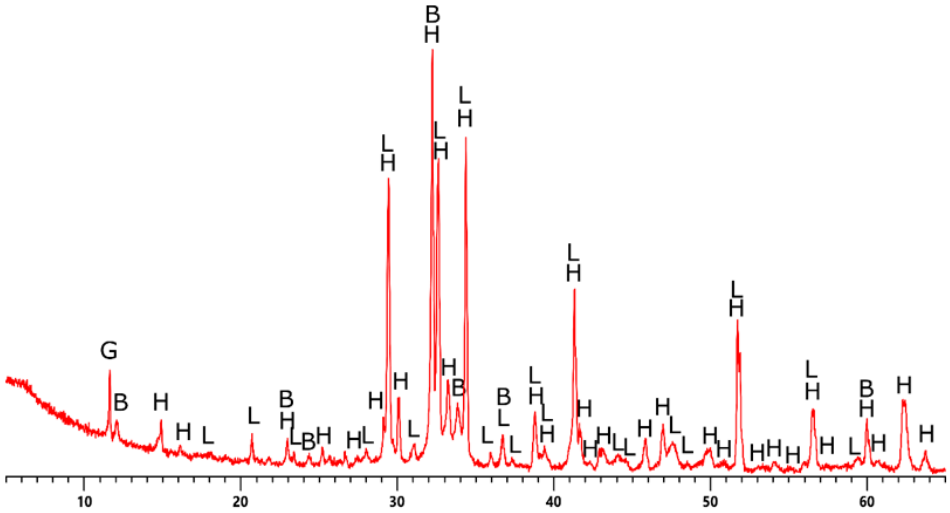

Figure 3. Phase analysis of CEM II A-S 52.5R cement (H—hatrurite, L—larnite, B—brownmillerite, G—gypsum).

The granulation of cement was measured via the laser diffraction technique and is presented in Figure 4. The particle size distribution (PSD) measurements were performed by the laser scattering method using the laser analyzer Horiba LA-300. The test involved passing laser beams through an isopropyl alcohol containing cement particles dispersed by ultrasounds and determining the particle size (in the range of 0.01–600 μm).

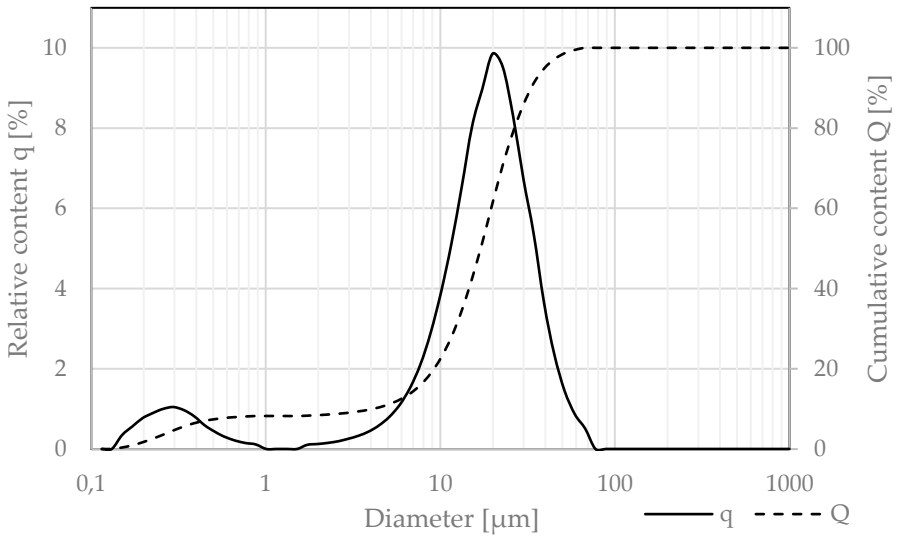

Figure 4. Relative (**q**) and cumulative (**Q**) granulation of CEM II/A-S 52,5R.

The nanoparticulate silica used in the study (Łaziska, Poland) met the requirements of EN 13263-1 [21]. Its specific surface area was measured via the BET method and was 23.86 m^2/g, with its adsorption isotherm as shown in Figure 5.

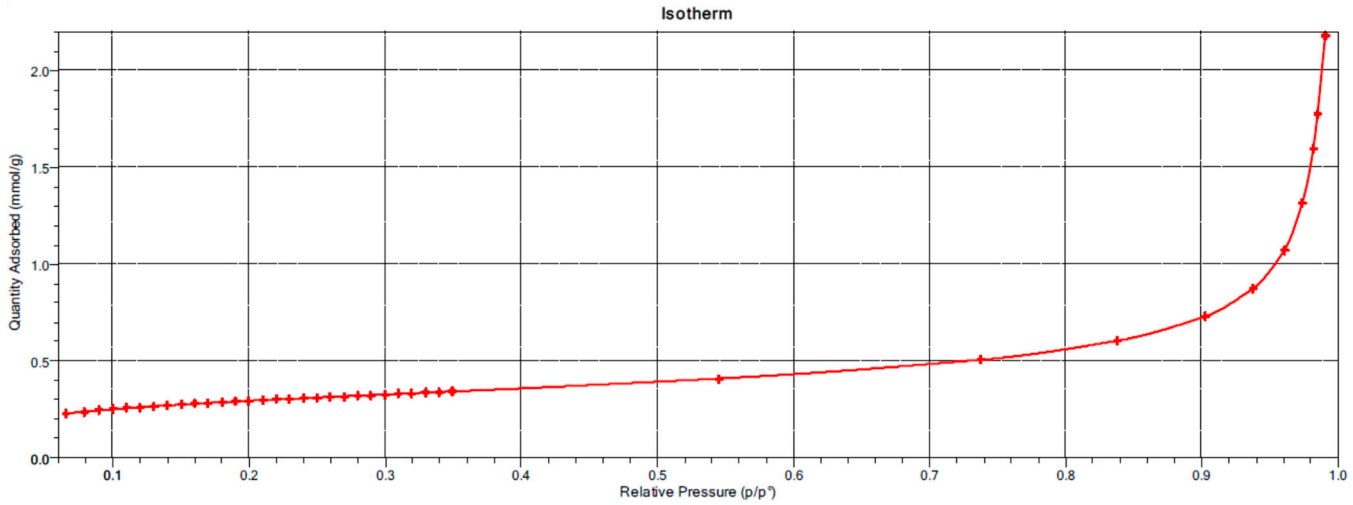

Figure 5. Adsorption isotherm of nanoparticulate silica.

The chemical composition of nanoparticulate silica was investigated via the XRF method, with the same test procedure as for the cement. The results are presented in Table 3.

Table 3. Summary of the results of the XRF analysis of nano-silica (%), LOI—loss on ignition.

MgO	Al_2O_3	SiO_2	P_2O_5	SO_3	Cl	K_2O	CaO	TiO_2	MnO	Fe_2O_3	CuO	ZnO	SrO	LOI
0.84	-	94.64	-	0.30	0.21	1.16	0.08	-	0.07	0.50	-	0.04	-	2.16

The analysis of the nanoparticulate silica activity index was carried out as per EN 13263-1 [21]. The results of the 28-day average compressive strength of the modified cementitious mortar (90% cement and 10% silica) and the results of the reference cementitious mortar are presented in Table 4.

Table 4. Strength tests of the 28-day mortar modified with nanoparticulate silica and the standard cementitious mortar CEM I 42.5R. The standard deviation is shown in parentheses.

Material	Compressive Strength after 28 Days (MPa)	Tensile Strength after 28 Days (MPa)	Activity Index after 28 Days (%)
Cementitious mortar modified with nanoparticulate silica	63.4 (±2.6)	11.5 (±0.3)	123
Reference cementitious mortar	51.5 (±1.5)	8.7 (±0.7)	-

The phase composition of nanoparticulate silica was investigated via the XRD method with the same test procedure as in the case of cement. The results are presented in Figure 6.

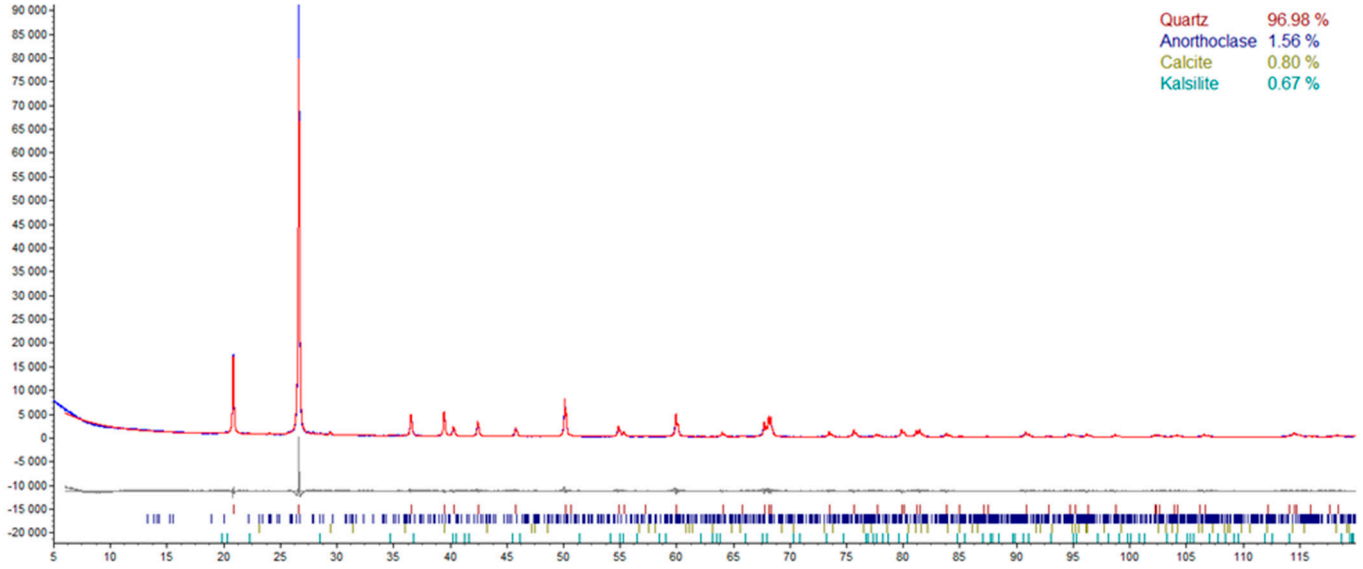

Figure 6. The quantitative phase composition of nanoparticulate silica.

The granulation of nanoparticulate silica was measured via the laser diffraction technique and presented in Figure 7, using the same test procedures as for the cement.

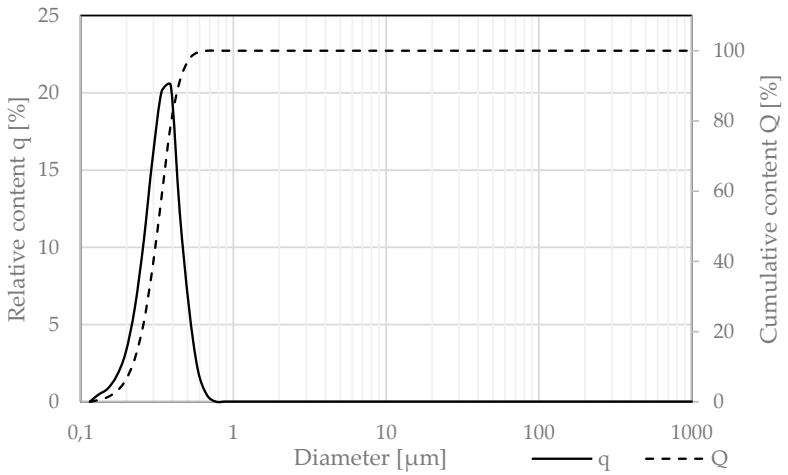

Figure 7. Relative (**q**) and cumulative (**Q**) granulation of nanoparticulate silica.

The quartz powder used in this study met the requirements of ISO/DIS 3262-13 [22]. Its granulation was measured via the laser diffraction technique and is presented in Figure 8, using the same test procedures as for the cement.

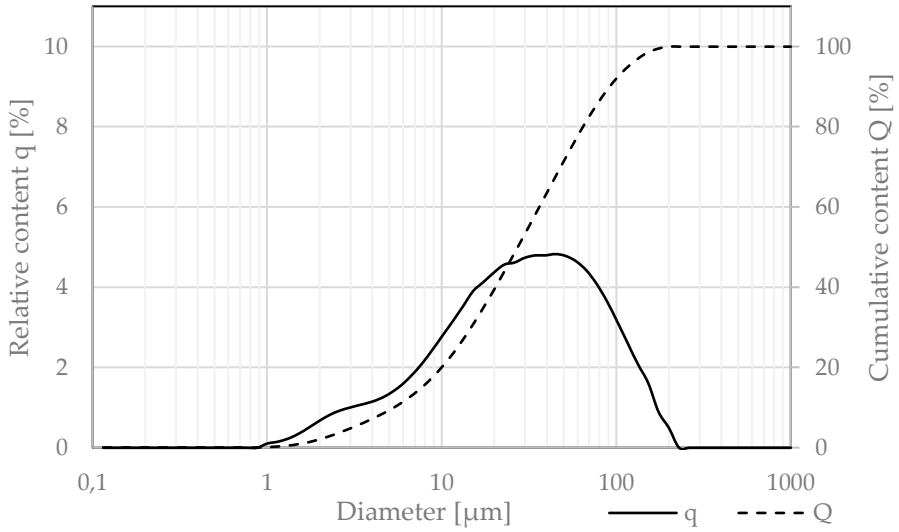

Figure 8. Relative (**q**) and cumulative (**Q**) granulation of quartz powder.

The study used two types of fire-dried quartz sand aggregates of different granulations: 0.1/0.5 and 0.5/1.2 (Corrado, Poland), which met the requirements of EN 13139 [23]. Table 5 lists their properties.

Table 5. Properties and composition of fire-dried quartz sand aggregates.

Property	Value	
Granulation	0.5/1.2	0.1/0.5
Dust content	0.1%	0.1%
Water absorption	0.1%	0.1%
SiO_2 content	99.4%	99.6%
Fe_2O_3 content	0.01%	0.01%
Al_2O_3 content	0.05%	0.06%
Solubility in water	0.0%	0.0%
Softening point	1582 °C	1506 °C
Sulfur content	<1%	<1%
Sand equivalent	99.17	99.06

This study used two types of titanium dioxide: TiO_2 (A)—K7000 (Leverkusen, Germany) and TiO_2 (B)—P25 (Shanghai, PRC), with properties in the powder state as described in [5]. The content of individual crystalline phases, the size of crystallites in tested samples, and the specific surface area of used materials are presented in Table 6.

Table 6. The content of individual crystalline phases and the size of crystallites in the tested samples were measured via XRD, and the specific surface area was measured via BET.

Photocatalyst	Phase (%)		Size of Crystallites (nm)		Specific Surface Area (m^2/g)
	Rutile	Anatase	Rutile	Anatase	
TiO_2 (A)	-	100	-	10	246.8 ± 2.9
TiO_2 (B)	13	87	54	33	53.8 ± 0.2

The chemical composition of titanium dioxides was investigated via the XRF method, with the same test procedure as for the cement. The results are presented in Table 7. The morphology of grains of both TiO_2 (A) and (B) is shown on SEM images in Figures 9 and 10.

Table 7. Summary of the results of the XRF analysis of titanium dioxides (%).

	Na_2O	SiO_2	P_2O_5	SO_3	Cl	TiO_2	Nb_2O_3
TiO_2 (A)	0.096	0.236	0.059	0.399	-	99.2	0.023
TiO_2 (B)	-	0.738	-	-	0.144	99.1	-

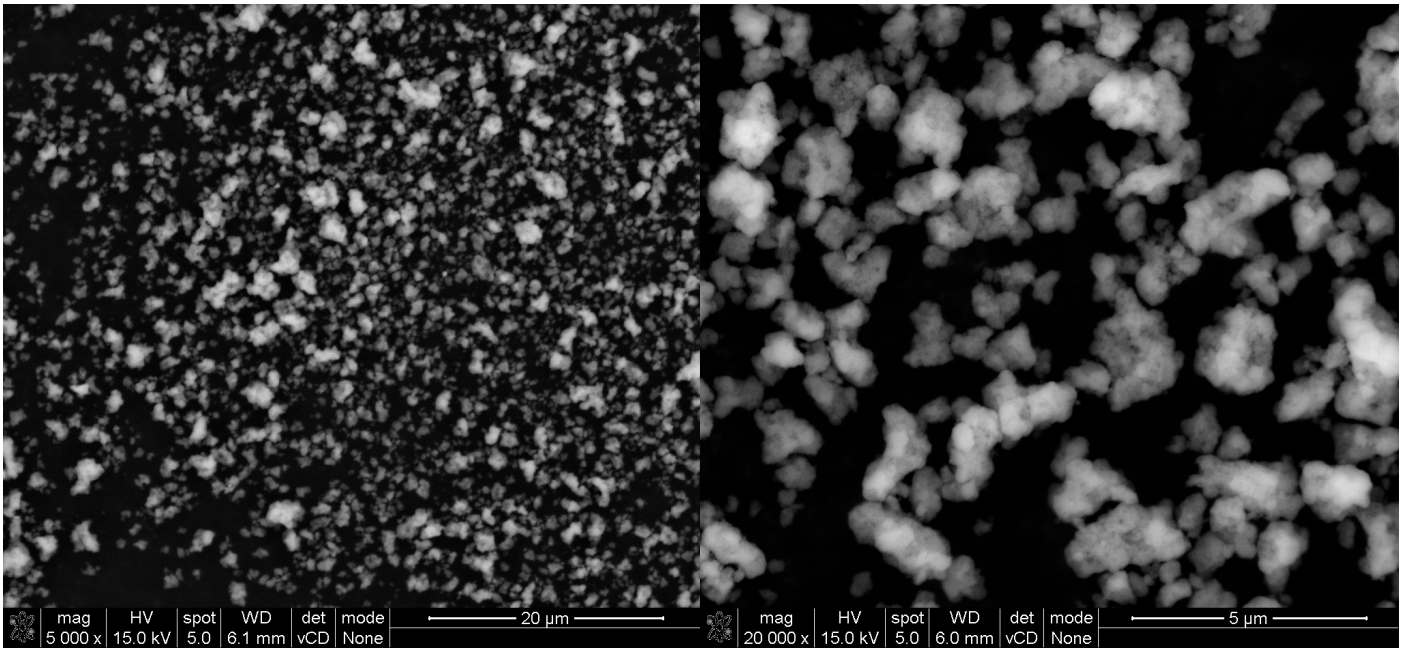

Figure 9. SEM (SE) micrographs of TiO_2 (A) under different magnifications.

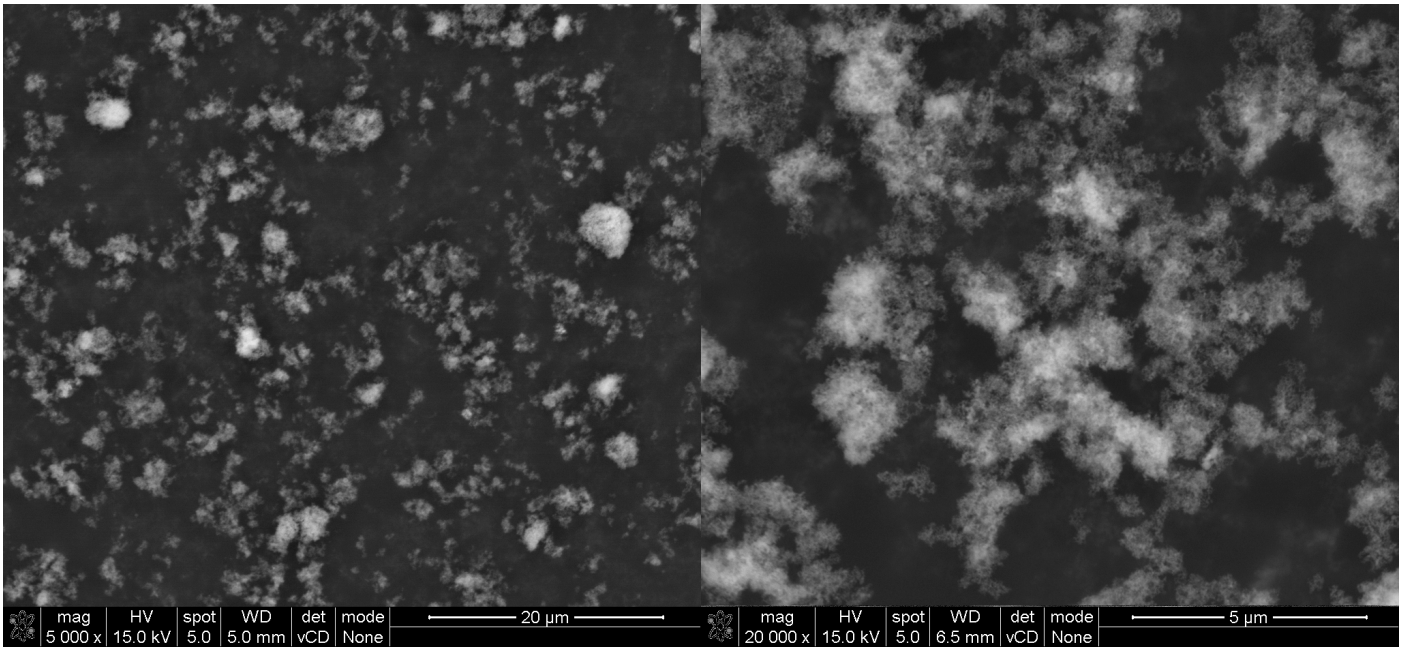

Figure 10. SEM (SE) micrographs of TiO_2 (B) under different magnifications.

The selected photocatalytic materials were introduced into the cementitious mortar as a dispersion made of a portion of mixing water and a PCE superplasticizer (polycarboxylate ether-based superplasticizer, referred to as SP), with of an electrostatic and steric mechanism of action and maximum suggested by the manufactured mass content at 3%m.c (Myślenice,

Poland). As titanium dioxide agglomerates in dry conditions, it was decided to use a sonicator to reduce the average TiO_2 grain size. Using a cavitation head, approx. 25 kJ of energy was introduced into every 250 mL of dispersion during a seven-minute cycle, consisting of 10 s steps (7 s of sonication followed by 3 s of pause).

The water used in this study met the requirements of EN 1008 [24]. An additional mass of superplasticizer was added to cementitious mortars to modify their rheological properties. It met the EN 934-2 standard [25] requirement and was characterized by electrostatic and steric mechanisms of action. In each prepared cementitious mortar, the total mass of the superplasticizer was set to 1% of the cement mass.

All described components were used to prepare cementitious mortars for the designed experiment plan. The composition of each of the prepared cementitious mortars is presented in Table 8.

Table 8. The composition of prepared cementitious mortars in the research plan.

Series ID		1	2	3	4	5	6	7	8	9–11
Component	**Unit**									
CEM II/A-S 52,5R		711	773	768	833	632	582	659	600	704
Water		306	332	269	292	272	250	231	210	275
Nanoparticulate silica		40	40	10	10	10	10	40	40	25
Quartz powder		125	41	136	44	33	103	35	106	78
Sand 0.1/0.5	kg/m^3	523	813	904	548	1065	685	694	1130	741
Sand 0.5/1.2		523	203	226	548	266	685	694	283	463
TiO_2 (A)		10	1	2.5	4	10	1	2.5	4	4.8
TiO_2 (B)		10	4	2.5	16	10	4	2.5	16	7.7
Superplasticizer (SP)		7.1	7.7	7.7	8.3	6.3	5.8	6.6	6.0	7.0

2.2. Methods

Designed cementitious mortars were prepared according to the mixing procedure described in EN 196-1 [26]. Before molding, the consistency of cementitious mortars was tested following the modified procedure based on EN 1015-3 [27]. A cone filled with fresh cementitious mortar was placed on the moistened plate, then removed to measure the flow diameter after one minute. The time for the fresh mortar to flow to the limit of 20 cm was also measured during the test to determine its viscosity. The VSI (Visual Stability Index) criteria according to ACI 237R-07 [28] were used to assess the degree of segregation.

After examining the consistency, samples were molded and stored for 24 h in a curing chamber (temperature 20 ± 2 °C, relative humidity RH ≥ 95%). After 24 h samples were demolded and cured in the curing chamber until further testing.

Tensile and compressive strength after seven days was tested according to the EN 196-1 [26] standard using three prism-shaped specimens with dimensions of 40 mm × 40 mm × 160 mm (with the latter halves of those prisms remaining after the three-point bending test).

The contact angle test was performed based on the BS ISO 27448 [29] standard on specimens with dimensions of 40 mm × 140 mm × 160 mm after 28 days of curing to investigate the self-cleaning properties of photocatalytic cementitious mortars. Before the test, samples were pretreated by dipping the tested surface in an n-heptane solution and drying at 70 °C for 15 min afterward. Samples were then set aside for 30 min to cool to room temperature. Next, the initial contact angle of distilled water was measured five times in different locations on a tested surface via a goniometer. Afterward, samples were placed in an irradiation chamber, where they were irradiated with UVA radiation (Philips BLB 8W fluorescent lamps) with an irradiation of 10 W/m^2 (Figure 11).

Figure 11. UV-A irradiation chamber with the distance between UV-A lamps and tested surface set in a way that irradiation of UV-A was 10 W/m^2.

The contact angle was then measured after 72, 74, and 76 h of sample exposure to UV-A radiation in five different locations on the tested surface. The test result was a percentage difference in the average initial contact angle and the average value of consecutive measurements after exposing the tested surface to UV-A radiation.

The self-cleaning properties of photocatalytic cementitious mortars were also tested via a rhodamine test based on UNI 11259 [30]. The test monitored the colorimetric changes of rhodamine drops on photocatalytic material subjected to UV radiation. On the tested surface, four spots were marked with a solution of rhodamine with water at a concentration of 0.1 g/1000 g. Each drop had a volume of 0.5 milliliters, following the UNI 11259 standard [30], and was measured with a single-channel automatic pipette. The samples were stored in the dark for 24 h until the drops were absorbed. After the drops were absorbed, an initial measurement was made using a spectrophotometer of the NS 810 series (Figure 12). Spectrophotometry is a technique to measure light absorption. It uses a light beam that passes through the sample, which absorbs or transmits light over a specific wavelength depending on its color. Data from the test can be used to determine sample color using various color spaces—in the case of the conducted research, the CIE Lab color scale.

Figure 12. Samples of photocatalytic cementitious mortars with drops of rhodamine and color testing using a spectrophotometer.

Two readings were taken for each droplet, i.e., for each surface, a total of 8 readings per sample. The factor tested was the change in the a* parameter, i.e., a component of the CIE L*a*b* color model: L* for lightness and a* and b* for the color opponents green-red and blue-yellow, respectively. The values of these three variables are usually absolute, with the L* value representing the darkest black at L* = 0 and the brightest white at L* = 100. On the other hand, the a* value represents red and green opponents at positive and negative values, respectively, and the b* value represents yellow and blue opponents at positive and negative values, respectively. The a* parameter indicates the intensity of the red color imparted to the samples by rhodamine staining. Its value is expected to decrease with time of exposure of photocatalytic material to UV-A radiation. After the initial measurement, samples were exposed to four hours of UV-A irradiation (Philips BLB 8 W fluorescent lamps) of 4 W/m^2 following UNI 11259 [30]. The same irradiation chamber was used as in the case of the contact angle test. However, the distance between UV-A lamps and the tested samples' upper surface was changed to acquire the required irradiation.

To determine the self-cleaning properties of photocatalytic cementitious mortars, it was investigated whether the measurement results followed the assumptions of UNI 11259 (Equations (4) and (5)) [30]. To characterize any surface with self-cleaning properties, the change in a* parameter after 4 h under UV-A radiation should be greater than 20% (R_4) and greater than 50% after 24 h (R_{24}). The a*(x) describes the reading on a* parameter with a spectrophotometer after irradiating samples for x hours in an irradiation chamber.

$$R_4 = \frac{a^*(0) - a^*(4)}{a^*(0)} \cdot 100\% \quad (4)$$

$$R_{24} = \frac{a^*(0) - a^*(24)}{a^*(0)} \cdot 100\% \quad (5)$$

The effectiveness of air purification from gaseous pollutants—nitrogen oxides—was carried out following the procedure developed as part of the project "Technology for the production of innovative self-cleaning prefabricated facade and surface elements that improve air quality", TECHMATSTRATEG-III/0013/2019. The test subject was photocatalytic cementitious mortar samples with dimensions of 40 mm × 140 mm × 160 mm. After demolding, the samples were cured for 28 days in a curing chamber. Before the test, the tested surface was cleaned of contamination. In the first step, the surface of the test sample was sprinkled with distilled water and scrubbed. Then, the sample was dried at 60 °C for two hours and placed in the irradiation chamber for 16 h with the test surface facing the light source, where the surface organic impurities were burned in UV-A radiation with an irradiance of 10 W/m^2. In the last step, the tested surface of the sample was cleaned

again with distilled water to remove impurities burnt out in the previous step and dried again at 60 °C for 2 h. The effectiveness of cleaning the air from gas pollutants was tested at the earliest two hours after the last drying cycle of the sample. Cleaned of impurities, the sample was placed in the glass reaction chamber, with the tested surface facing the light source. The glass reaction chamber was tightly closed and sealed (Figure 13). UV-A LED strips (360 ± 5 nm, 14.4 W/m) were used as a UV-A light source, and Sun-Like™ TRI-R™ LED strips (5000 K) were used as a visible light source. The UV-A and UV-B irradiation of the visible light source on the sample's surface was 0.0 W/m^2, and the global irradiation was 150 W/m^2. The UV-B irradiation of the UV-A light source on the sample's surface was 0.0 W/m^2, and the global irradiation was 1.2 W/m^2. UV-A and UV-B irradiations were measured using Delta Ohm pyranometers: UV-A (315–400 nm) and UV-B (280–315 nm). The global irradiation was measured using a Lambrecht METEO pyranometer in the range of 285–3000 nm. The temperature in the glass reaction chamber during the experiment was kept at a value of 25 ± 3 °C, and relative humidity at a value of 40 ± 5%. The gas flow was kept at a constant value of 2 L/min.

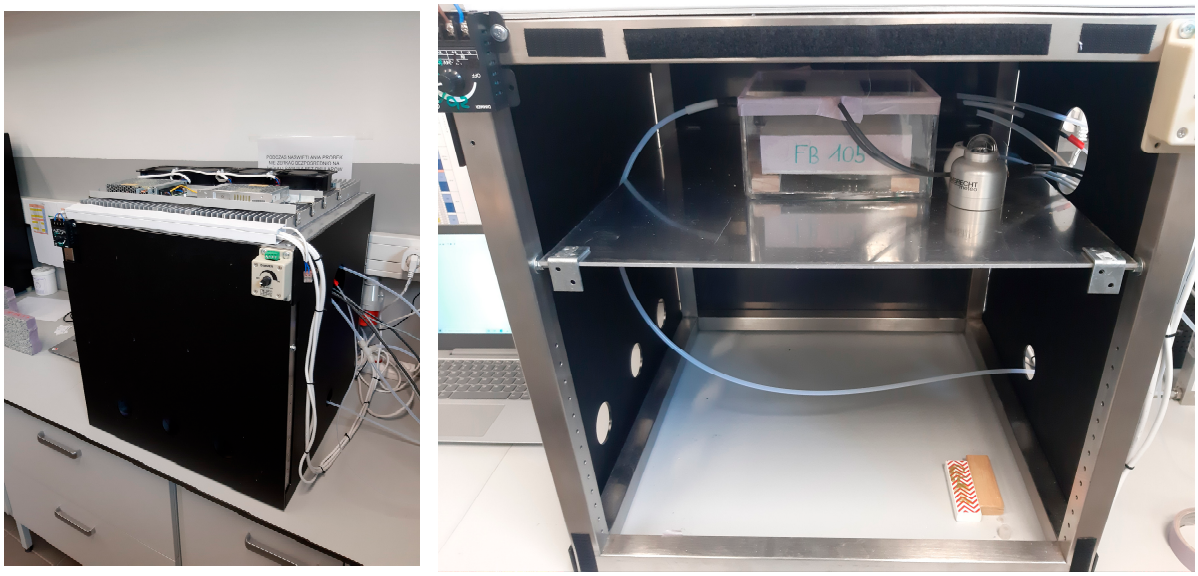

Figure 13. A glass reaction chamber with a photocatalytic sample. The measuring station was enclosed with shields impenetrable to UV-A and TRI-R radiation.

The quantification of the results (the concentration of NO and NO_x) was conducted using the Teledyne API T200 chemiluminescence detection analyzer (San Diego, CA, USA). The analyzer was characterized by a lower detectable limit of 0.2 ppb (maximal 20,000 ppb), with the precision of analysis listed as 0.5% of reading value, and the zero noise below 0.1 ppb, with expanded relative uncertainty of 9% (taking into consideration all elements of analytical setup).

The study consisted of several stages (Figure 14), i.e.,

1. Filling the reaction chamber with nitrogen oxides to achieve its concentration of 100 +/− 5 ppb;
2. Irradiation of the sample with UV-A light with an irradiance of 0.2 W/m^2 and measurement of the concentration of nitrogen oxides while maintaining the gas flow from the first step;
3. Measurement of the concentration of nitrogen oxides after switching off the light source, while maintaining the gas flow from step one;
4. Emptying the reaction chamber of nitrogen oxides;
5. Filling the reaction chamber with nitrogen oxides to achieve its concentration of 100 +/− 5 ppb;

6. Irradiation of the sample with visible light with an irradiance of 150 W/m^2 and measurement of the concentration of nitrogen oxides, while maintaining the gas flow from the first step;
7. Measurement of the concentration of nitrogen oxides after switching off the light source, while maintaining the gas flow from step one;
8. Emptying the chamber of nitrogen oxides;
9. Filling the reaction chamber with nitrogen oxides to achieve its concentration of 100 +/− 5 ppb;
10. Irradiation of the sample with UV-A light with an irradiance of 0.2 W/m^2 and visible light with an irradiance of 150 W/m^2 and measurement of the concentration of nitrogen oxides, while maintaining the gas flow from the first step;
11. Measurement of the concentration of nitrogen oxides after switching off the light source, while maintaining the gas flow from step one;
12. Emptying the chamber of nitrogen oxides.

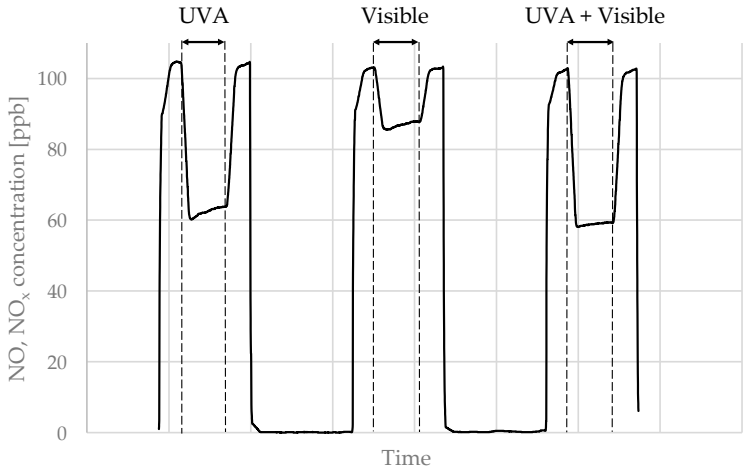

Figure 14. A schematic for the performed test procedure of air purifying test for cementitious mortar 4.

The nitrogen oxide concentration was approximately 100 ppb to model the actual NO_x concentration in the urban environment. UV-A and visible light irradiance were chosen as 0.2 and 150 W/m^2 to model the actual summer solar radiation conditions in the Polish territory (UV index of 8–9 and visible light irradiation of 1000 W/m^2–150 W/m^2 were the maximal settings of the testing apparatus).

3. Results

The results of the consistency tests of prepared photocatalytic cementitious mortars are presented in Table 9. It was found that prepared cementitious mortars differed in rheological properties in a selected range of variables. Depending on the mortar composition, its free flow varied significantly, within the range of 160 to 375 mm (the mass amount of superplasticizer was the same in all prepared series). In only two prepared series, visual signs of segregation were observed. The time required for the sample to flow to 200 mm was comparable between most prepared cementitious mortars, except for mortar 8, which was characterized by too high viscosity to reach the flow of 200 mm.

Table 9. VSI segregation, t_{20}, and consistency of tested cementitious mortars.

Series ID	VSI	t_{20} (s)	Flow Diameter (mm)
1	0	1.0	310
2	2	1.0	375
3	1	1.0	355
4	0	1.0	330
5	0	2.0	275
6	0	2.0	300
7	0	2.5	305
8	0	-	160
9	0	1.5	300
10	0	2.0	280
11	0	2.0	290

Mechanical strength tests after seven days of curing also showed significant differences (Figure 15). The tensile strength for all series was in the range of 6.19 MPa (mortar 11) to 8.15 MPa (mortar 4). For compressive strength, the difference between different series was more significant—the mortar with the lowest compressive strength was mortar 11 (55.77 MPa), and the highest was mortar 3 (77.7 MPa).

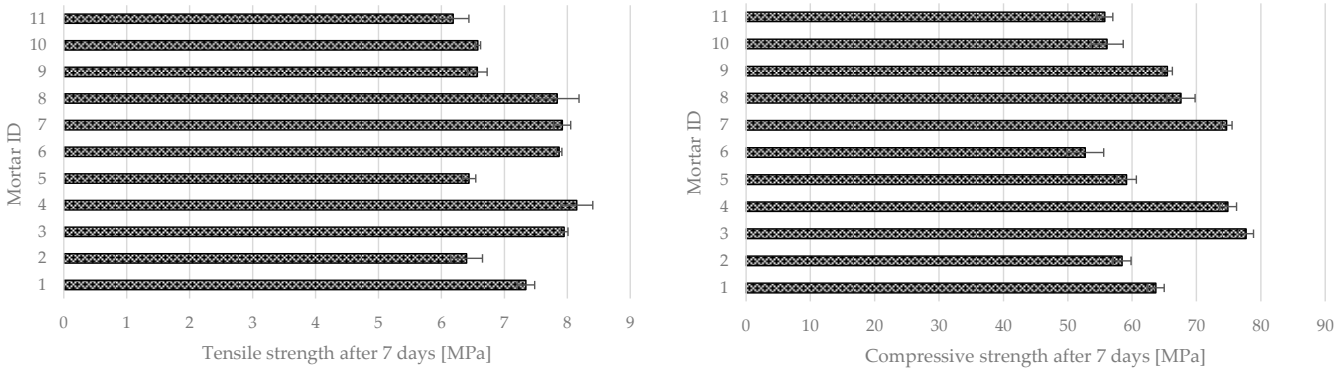

Figure 15. Tensile (**left**) and compressive (**right**) strength of photocatalytic cementitious mortars after seven days of curing.

The results of the self-cleaning tests via the rhodamine test are presented in Figure 16. For the surface of the material to be described as self-cleaning, the reduction in parameter a should be at least 20% after four hours of irradiating in UV-A light of a given irradiation and at least 50% after 24 h. In the case of the prepared photocatalytic cementitious mortars, the R4 value varied significantly, ranging from −1.49% for mortar 7 to −30.88% for mortar 1. Out of the 11 prepared series, only six were characterized with an R4 parameter greater than −20%. The R24 value also varied significantly, ranging from −7.31% for mortar 7 to −58.23% for mortar 9. Out of the 11 prepared mortars, only three were characterized with an R24 parameter greater than 50%. Based on the experiment, out of the 11 prepared mortars, only three surfaces could be described as self-cleaning ones.

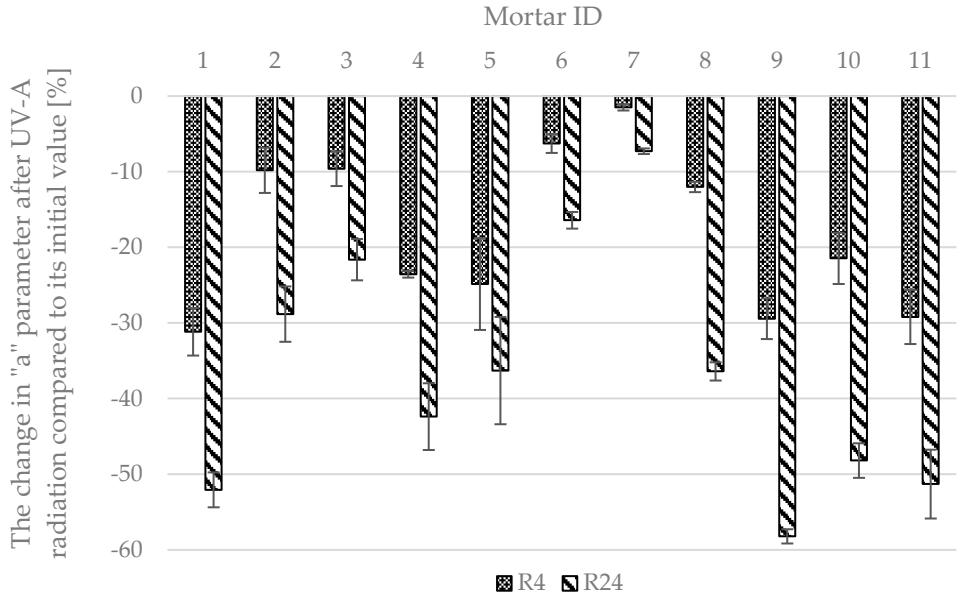

Figure 16. Results of self-cleaning test for photocatalytic mortars via rhodamine test.

The results of self-cleaning tests via the contact angle test are presented in Figure 17. The limit value for this test is not specified in BS ISO 27448 [28]. In the case of the prepared photocatalytic cementitious mortars, the change in contact angle caused by UV-A irradiation varied significantly, ranging from −17.7% for mortar 10 to −35.0% for mortar 1. Out of the 11 prepared mortars, only seven were characterized by a reduction in contact angle greater than 25%. Figure 18 presents the actual data that was analyzed to calculate the contact angle in any test measurement.

The test results of the effectiveness of air purification from gaseous pollutants—nitrogen oxides—are presented in Figure 19. The result of any given test regarding air purification efficiency was a relative reduction in the concentration of both NO and NO_x under different irradiation conditions compared to its initial concentration with UV-A or visible light lamps turned off.

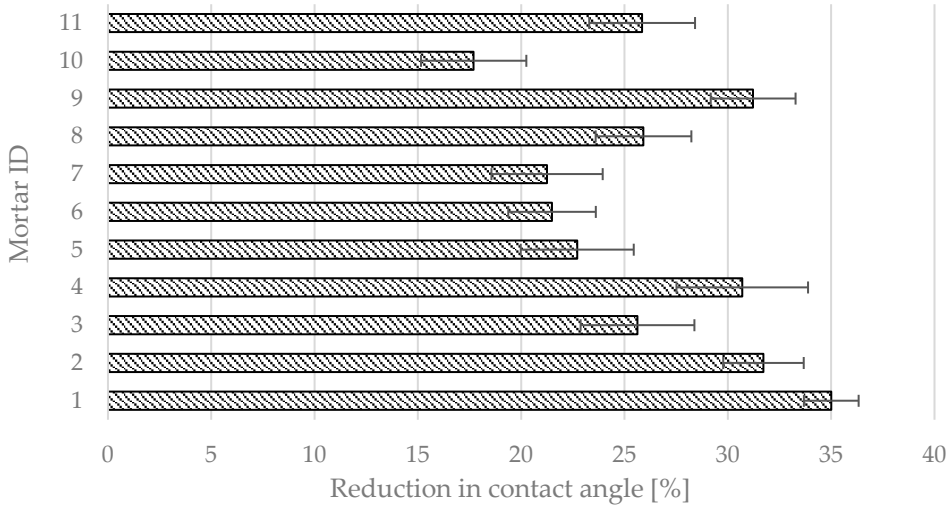

Figure 17. Results of self-cleaning test for photocatalytic cementitious mortars via contact angle test.

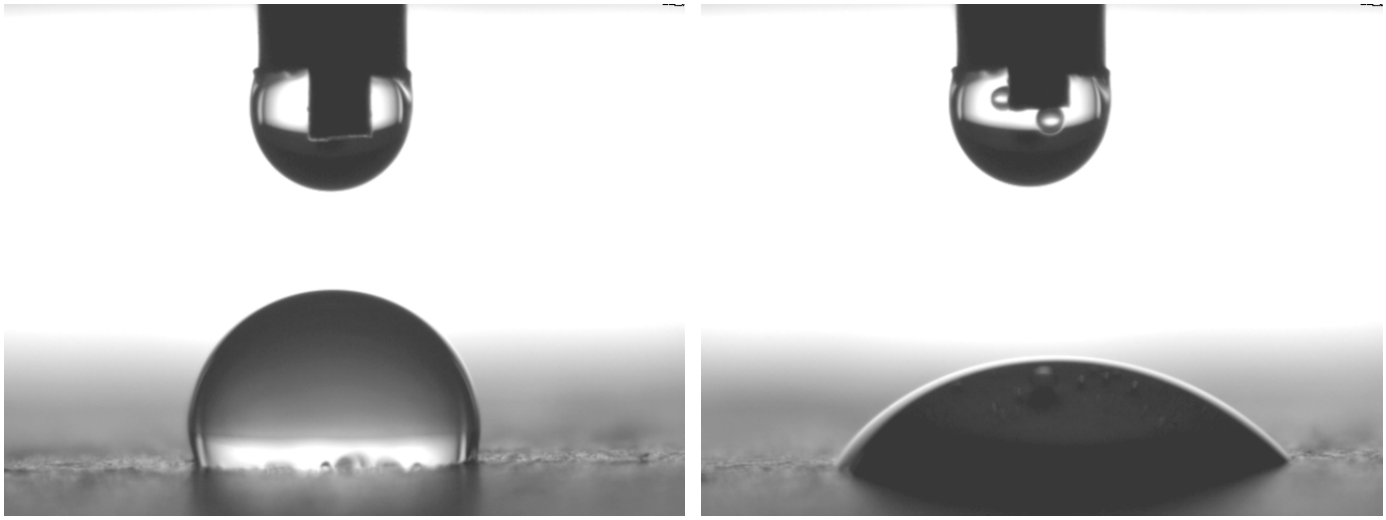

Figure 18. The contact angle between the self-cleaning surface and the drop of distilled water. The photograph to the left shows the initial contact angle and to the right after 72 h of UV-A radiation for the photocatalytic mortar 4.

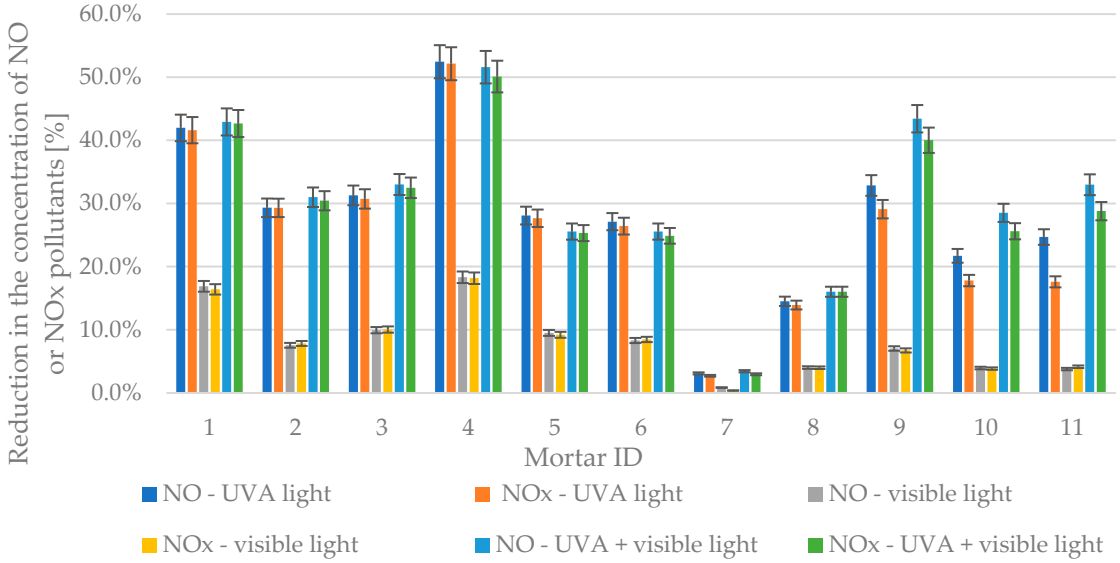

Figure 19. Reduction in the concentration of NO or NOx pollutants in different types of radiation.

In the case of the prepared photocatalytic cementitious mortars, the reduction in concentrations of both NO and NO_x varied significantly between different series and in various types of radiation present (UV-A, Visible, or both). The lowest reduction in all irradiation environments was observed for mortar 7—for UVA reductions were 3.1% and 2.7% for NO and NOx respectively, for TRI-R reductions in pollutant concentrations were 0.9% and 0.4% for NO and NOx respectively, and for combined UVA and visible light reductions were 3.4% and 3.0% for NO and NOx, respectively. The highest reductions in nitrogen oxides were observed for mortar 4—for UVA reductions were 52.4% and 52.1% for NO and NOx, respectively, for TRI-R reductions in pollutants concentrations were 18.3% and 18.2% for NO and NOx, respectively, and for combined UVA and TRI-R reductions were 51.6% and 50.1% for NO and NOx, respectively.

4. Discussion

The prepared research plan aimed to investigate the influence of selected material variables on the properties of photocatalytic cementitious mortars. Several variables were

considered, representing the components of regular mortars and photocatalytic additives. It was found that each of the assumed variables, in the assumed range of variability, significantly influenced at least one of the tested properties of photocatalytic materials (Table 10). The analysis of obtained test results was conducted via screening design using the Plackett–Burman method, a bivalent elimination plan with a triply repeated central point, where each of the considered variables has an average value from an assumed range of variability. In this type of statistical plan, statistically significant variables for tested properties can be identified with a reduced number of required samples. In the conducted research, seven different variables were considered. A photocatalyst must be included in its composition to obtain a cementitious material with photocatalytic properties [31]. As it represents an additional component of the mix, it is proper to assume it will also influence other material properties [32].

Table 10. Summary of statistically significant variables on studied properties of photocatalytic cementitious mortars based on Pareto charts with the assumption of $p = 0.05$ (gray color indicates the non-significant influence of selected variables on tested property).

Property	Statistically Significant Variables						
	b/s	w/c	TiO_2 (A)/TiO_2 (B)	Nanoparticulate Silica	Quartz Powder	TiO_2 Mass	Sand Ratio
Consistency (mm)	+				-	-	
t_{20} (s)	-	-	-	+	+	+	-
VSI (-)	+					-	-
Tensile strength (MPa)		-					+
Compressive strength (Mpa)	+	-					
Rhodamine—4 h—reduction in "a" parameter (%)	+	+				+	
Rhodamine—24 h—reduction in "a" parameter (%)	+	+				+	
Reduction of contact angle (%)	+	+	-	+		+	
NO—UVA light (%)	+			-		+	
NO—visible light (%)	+			-		+	
NO—UVA+visible light (%)	+			-		+	
NO_X—UVA light (%)	+			-		+	
NO_X—visible light (%)	+			-		+	
NO_X—UVA+visible light (%)	+			-		+	

Although the total mass of titanium dioxides in the performed study was 5 to 20 kg/m^3, even such a small content compared to the mass content of other components had a thickening effect on the consistency of fresh mortar (Figure 20). It was found that consistency-wise, the increase in the ratio between the binder (cement+quartz powder to sands) had a fluidizing effect on fresh mortar. This observation is logical, as the superplasticizer (SP) content depended on the mass of cement in the mix—with an increase in the b/s ratio, the mass of cement increased and, therefore, the SP mass amount. On the other hand, by increasing the b/s ratio, the amount of cement paste within the mortar increases, and the amount of sand aggregate decreases; this dependence also contributes to an increase in mortar fluidity. Additionally, with an increase of quartz powder replacing cement, the thickening effect on mortar's consistency was observed, linked with an increased water demand of fine aggregate. The observation regarding titanium dioxide content regarding rheological properties of cementitious materials was compliant with the scientific literature on the subject [33]. TiO_2 is characterized by fine granulation, depending on the efficiency of the breakdown of agglomerates with, for example, ultrasounds—in extreme conditions, its granulation could be reduced to crystallite size (10–100 nm). By introducing such a fine component into the mix, its rheology is going to be impacted.

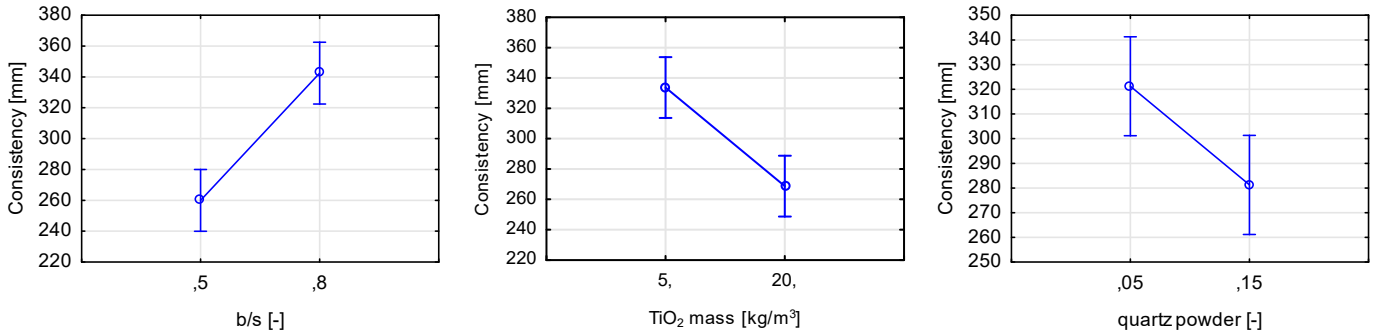

Figure 20. Marginal mean charts for statistically significant variables for consistency of prepared cementitious mortars in order of significance from the left—b/s ratio, TiO_2 mass content, and the replacement percentage of cement with quartz powder.

The segregation of individual components of fresh mortar is closely linked with its rheological properties [34]. If the yield stress of fresh mortar is high, it is characterized by low consistency. In addition, as its plastic viscosity increases, the time required to reach a specific flow increases. In the conducted study, the time required for the fresh mortar to flow to a diameter of 200 mm was measured—an indirect study on the influence of selected variables on the viscosity of fresh mortars. All assumed variables in the assumed range of variability had a statistically significant effect on the rheological properties of fresh mortars (Figure 21). In this graph, the effect ratings obtained by the ANOVA procedure are ordered from the highest absolute value to the lowest. The value of each effect is represented by a bar and a line that indicates how large the effect should be to be statistically significant (in the conducted research, the *p*-value was chosen at a standard value of 0.05).

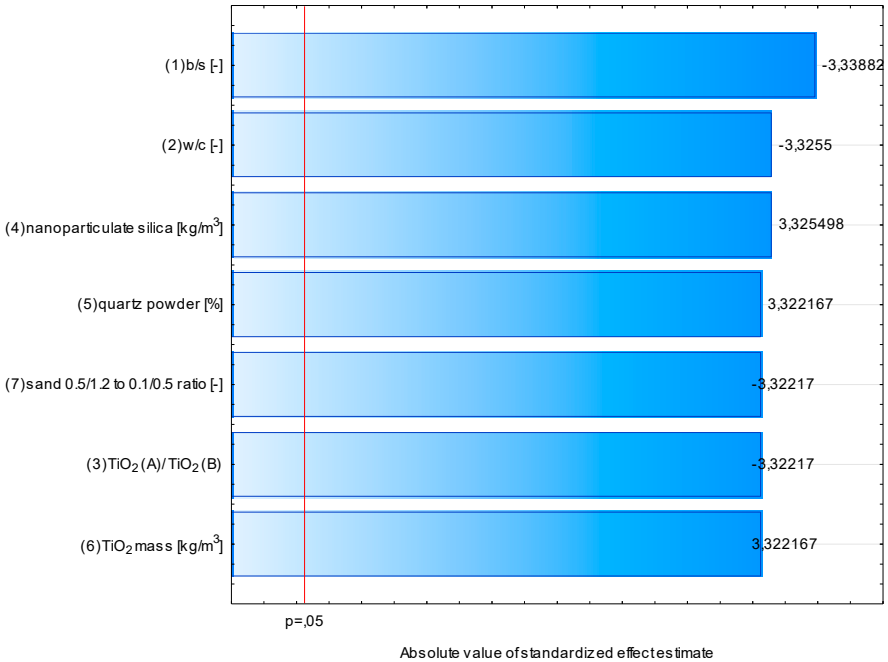

Figure 21. Pareto chart of the absolute value of standardized effect estimate of variables considered in the study on the t_{20} parameter.

An increase in TiO_2, nanoparticulate silica, and quartz powder content caused an increase in the viscosity of fresh mortars. On the other hand, an increase in b/s, w/c, and sand ratio had the opposite effect. The thickening effect was due to an increase in fine grains in the mortar, regardless of their material origin [35]. In the case of variables contributing to an increase in fluidity, the change was caused by either the increase in cement paste content

of low viscosity (due to its modification with SP), an increase in water content (fluid of low viscosity), or an increase in the content of coarser-grained sand aggregate (0.5/1.2). The VSI (Visual Stability Index) value for all prepared mortars was investigated as part of the research. This method assumes grading the visual quality of a fresh mortar on a scale of 0 to 3, where 0 is no segregation and 3 is extreme segregation of fresh mortar. It was found that three out of seven considered variables influenced this property (Figure 22). However, out of the 11 prepared mortars, only two were characterized with a VSI higher than 0.

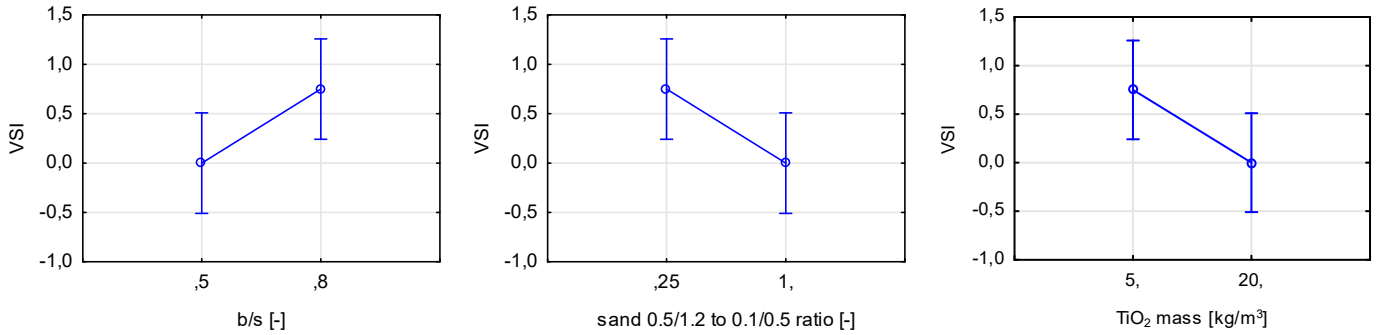

Figure 22. Marginal mean charts for statistically significant variables for VSI of prepared mortars in order of significance from the left—b/s ratio, the ratio between sands 0.5/1.2 and 0.1/0.5, and TiO_2 mass content.

In the assumed range of variability, TiO_2 mass content did not influence the mechanical properties of hardened mortars after seven days of curing. The significant variables in the case of compressive strength were the water-to-cement ratio and binder-to-sand ratio, and in the case of tensile strength, the water-to-cement ratio and ratio between two used sands (Figure 23). For compressive strength, an increase in the b/s ratio also increased the strength of the material. For tensile strength, an increase in the content of coarser sand aggregate contributed to an increase in strength.

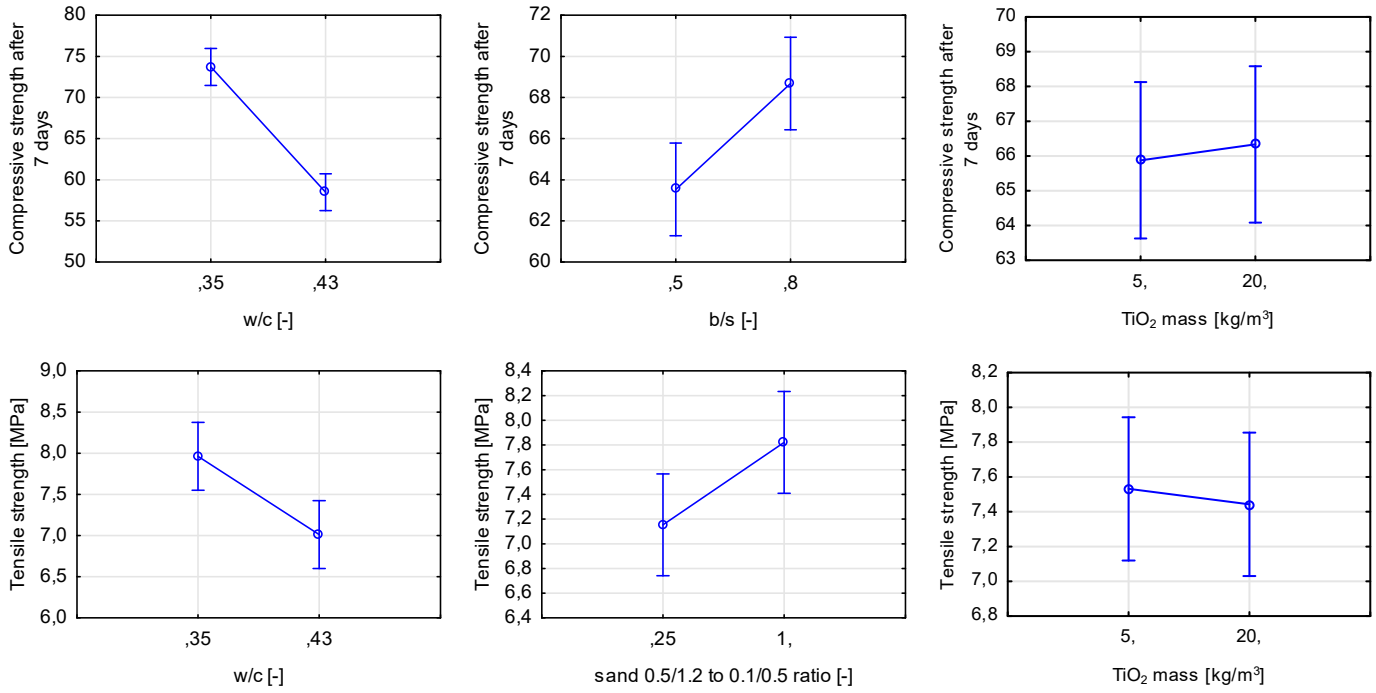

Figure 23. Marginal mean charts for statistically significant variables for compressive and tensile strength of hardened mortars after seven days of curing in order of significance from the left—w/c ratio

and b/s ratio for compressive strength and w/c ratio and ratio between sands for tensile strength. The last graph for both compressive strength and tensile strength shows an influence of one of non-significant variables—TiO_2 mass content.

Overall, TiO_2 addition influenced the properties of fresh mortar; however, it did not significantly contribute to any changes regarding the mechanical properties of the composite. In scientific literature, it is reported that a higher mass amount of TiO_2 in the cementitious composite can act as an ultra-fine aggregate, increasing the material's mechanical properties [18,36].

The most critical information from the conducted research was that TiO_2 mass is not the only and not the most statistically significant variable concerning the air purification from nitrogen oxides and the self-cleaning properties of tested cementitious materials. TiO_2 content was the second or third most significant variable in the considered range of variability, depending on the tested property. In each case, the increase in its mass content was equivalent to a rise in photocatalytic efficiency, either measured by air purification tests or self-cleaning ones.

For all air purification tests, regardless of the type of nitrogen oxide content being measured (NO or NO_x), three variables proved to be statistically significant. Binder-to-sand ratio proved to be the most significant, contributing in each test to an increase in the efficiency of air purification (Figures 24 and 25).

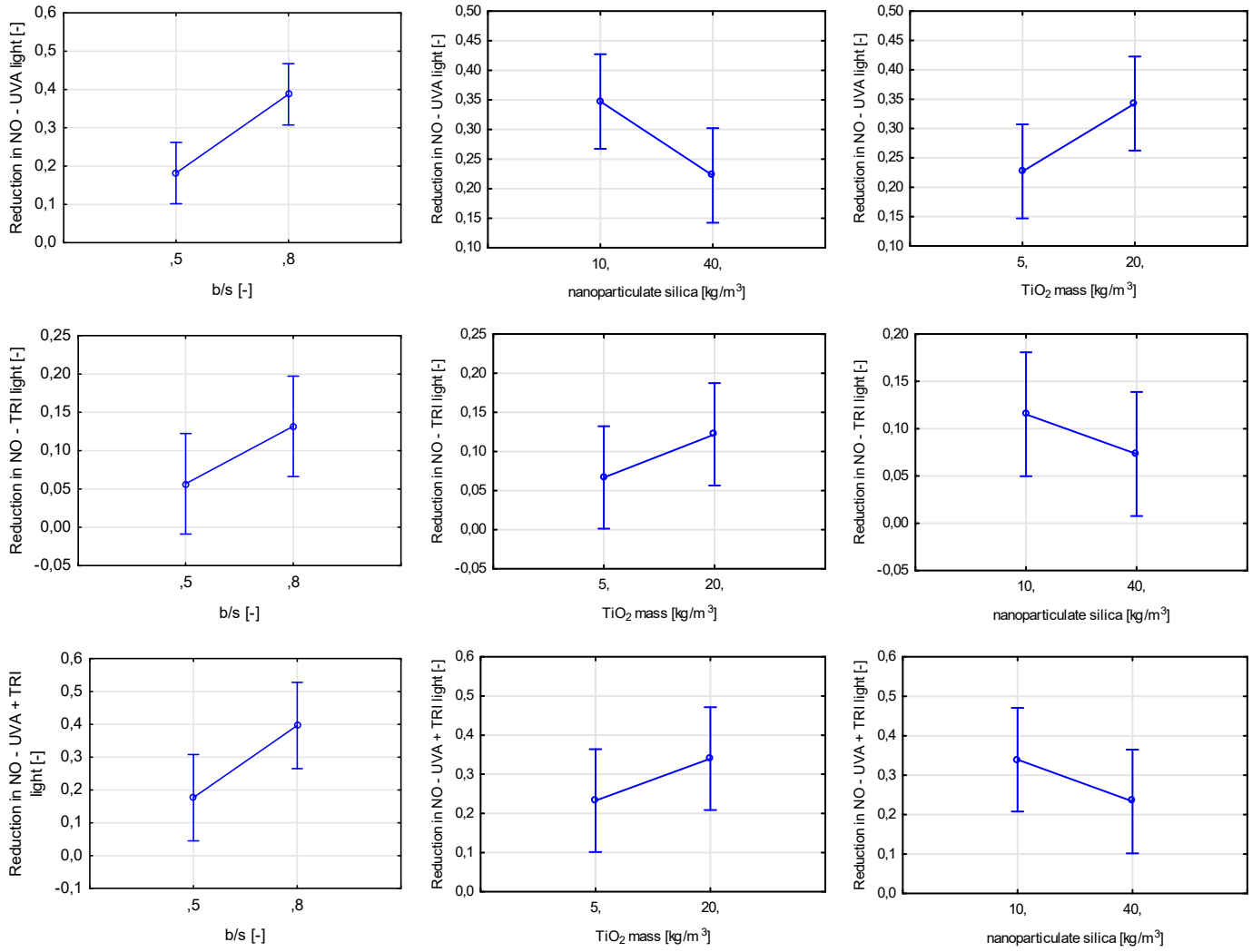

Figure 24. Marginal mean charts for statistically significant variables for efficiency in air purification from NO under different light sources (UVA light, visible light (TRI), UVA + visible light) in order of

significance from the left—b/s ratio, nanoparticulate silica mass content, and TiO_2 mass content for UVA light and b/s ratio, TiO_2 mass content, and nanoparticulate silica mass content for both visible light and UVA + visible light.

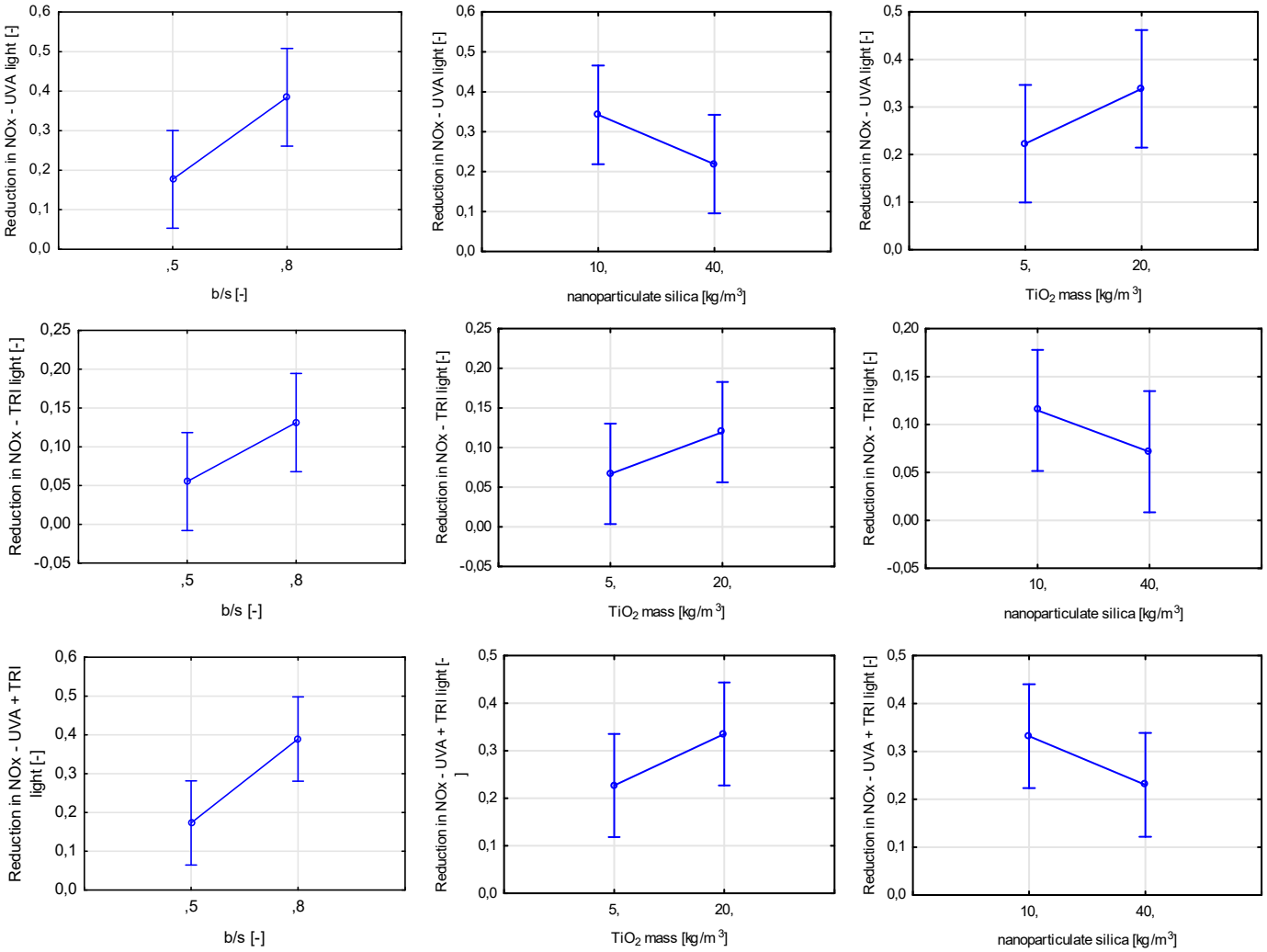

Figure 25. Marginal mean charts for statistically significant variables for efficiency in air purification from NO_x under different light sources (UVA light, visible light (TRI), UVA + visible light) in order of significance from the left—b/s ratio, nanoparticulate silica mass content and TiO_2 mass content for visible light and UVA + visible light, b/s ratio, TiO_2 mass content, and nanoparticulate silica mass content for UVA light.

It is well-established that incorporating photocatalytic materials in the composition of cementitious materials is the sole reason for the material to gain photocatalytic properties [8,19,30]. However, the remaining components of the mix impact the distribution of TiO_2 within the cement matrix. From the conducted research, a conclusion can be drawn that in the selected range of variability of mass content of titanium dioxide in the mortar, the composition of mortar significantly impacts the properties regarding air purification. With an increase in the binder-to-cement ratio of the material, the volume in which TiO_2 has distributed increases, reducing its chance to agglomerate and increasing the surface on which photocatalytic reactions can occur (Figure 26). In addition, TiO_2 particles can act as crystallization nuclei for hydration products. With an increase in the b/s ratio of the mortar, the phenomenon of self-drying of the cement matrix is intensified, limiting its hydration degree and the number of TiO_2 particles being wholly covered with hydration products.

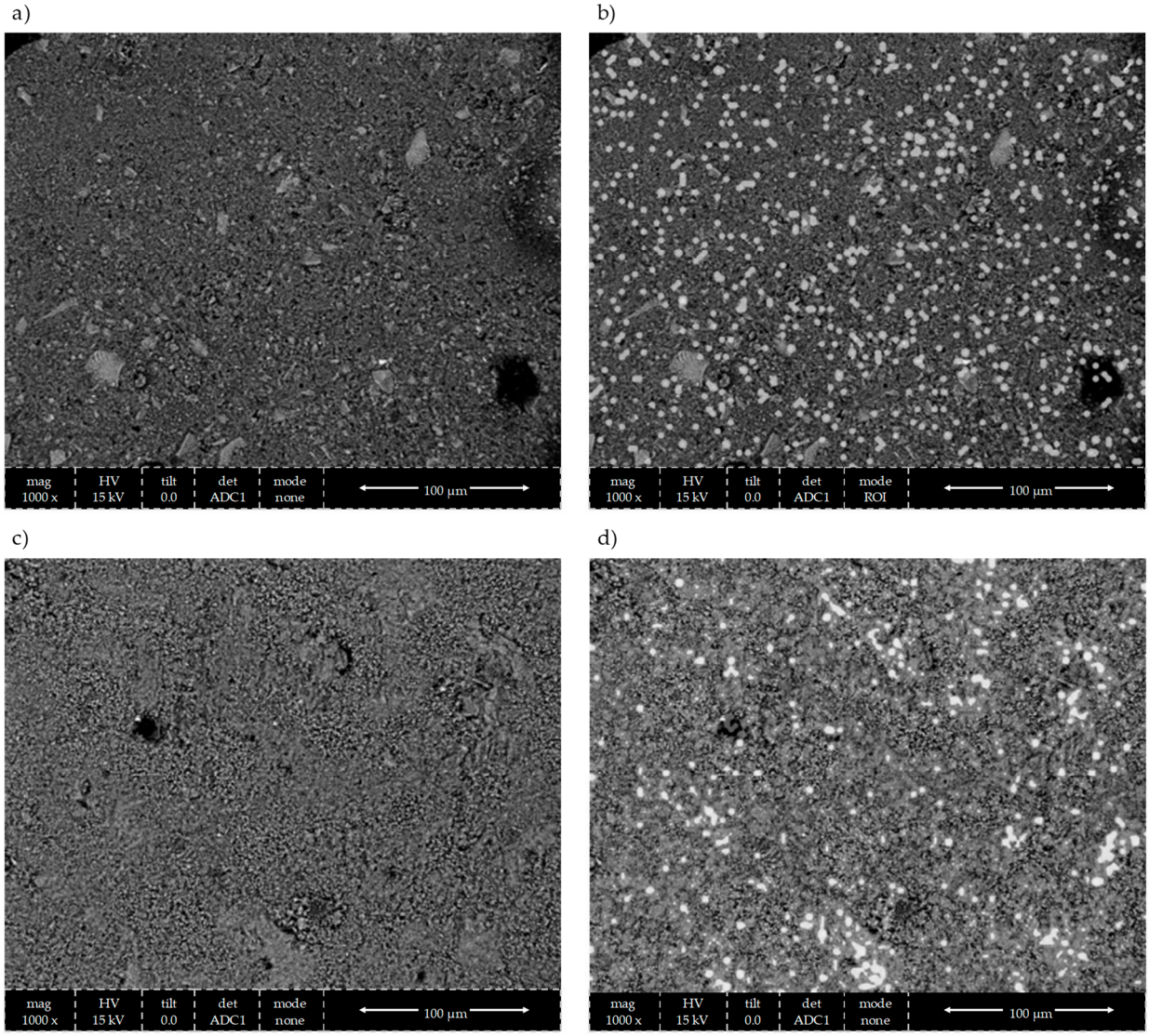

Figure 26. Agglomeration phenomenon of TiO_2 grains—SEM (SE) micrographs of the surface of prepared mortars with EDS mapping of qualitative imaging of TiO_2 presence: (**a**) SEM (SE) of mortar of b/s = 0.8; (**b**) SEM (SE) with EDS mapping of TiO_2 (white grains) of mortar of b/s = 0.8; (**c**) SEM (SE) of mortar of b/s = 0.5; (**d**) SEM (SE) with EDS mapping of TiO_2 (white grains—agglomerates) mortar of b/s = 0.5.

The effect of nanoparticulate silica was opposite to that of the b/s ratio, as it is a component of the mix added to increase the tightness of the material and acts as an ultra-fine filling material, reducing the exposure of titanium dioxide to sun radiation. Interestingly, changes in the water-to-cement ratio did not contribute to the difference in the efficiency in purifying the air from NO and NO_x, suggesting that either its variability was chosen in too narrow a scope or that the porosity of the cement matrix has a negligible effect on the intensity of photocatalytic reactions.

The rhodamine test also singled out three variables having a significant influence on the self-cleaning properties of the material (Figure 27). The total mass content of titanium dioxide was the most statistically significant, followed by the binder-to-sand ratio and the water-to-cement ratio. Contrary to air purification tests, an increase in the porosity of the cement matrix caused by an increase in the water-to-cement ratio led to an increase in the self-cleaning properties of prepared mortars. A drop of rhodamine solution or water is placed directly on the tested surface in both the rhodamine test and the contact angle test. Properties of that surface influence the initial size of the contact plane between the

object whose properties are tested (contact angle for the drop of water, change in color for rhodamine). In the case of air purification tests, the influence of surface properties is slimmer and comes down to the surface covered in TiO_2, as gaseous pollutants need to be in contact with the photocatalyst physically.

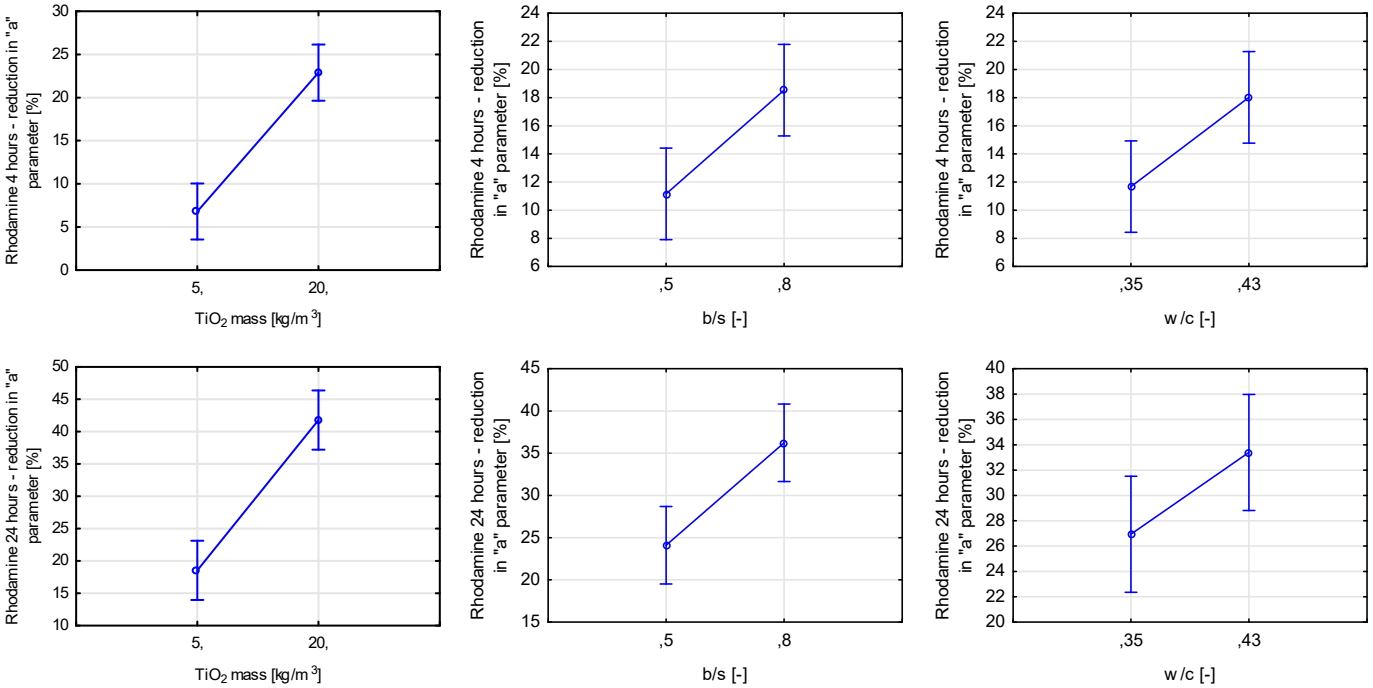

Figure 27. Marginal mean charts for statistically significant variables for self-cleaning via rhodamine test after 4 and 24 h of radiating samples with UVA light in order of significance from the left—TiO_2 mass content, b/s ratio, and w/c ratio.

The binder-to-sand ratio also influenced the material's ability to self-clean tested via the rhodamine test. As shown before, an increase in its value contributes to an increase in the composite's ability to purify the air from pollutants. It is safe to assume that due to better dispersion of titanium dioxide within the cement matrix in the case of increasing b/s ratio value, better exposure of TiO_2 grains to the radiation source was obtained, increasing materials' self-cleaning properties.

Finally, the final self-cleaning test concerning the change in the contact angle between a drop of distilled water and the tested surface showed a statistically significant influence of five assumed variables (Figure 28). The most significant of them was the binder-to-sand ratio, followed by TiO_2 content and nanoparticulate silica mass content. All of the significant variables influenced the contact angle reduction after exposure to UVA radiation, except the ratio between the two photocatalysts used in the study. As in the rhodamine test, the properties of the tested surface, except the TiO_2 content, influenced the course of the test.

Out of the seven included variables, three did not influence the air purification and self-cleaning properties of photocatalytic mortars—the replacement level of cement with quartz sand, the sand ratio, and the mass ratio between two photocatalysts. In the case of quartz powder, the range of variability was probably too narrow. Even if that was the case, the information that part of cement can be replaced with a material with a significantly lower carbon footprint without compromising its photocatalytic properties presents a vital conclusion from the performed research. The assumed variability of mass ratio between two sands of different granulations was wide; however, it did not affect the photocatalytic properties of prepared mortars. This phenomenon could be related to the amount of cement paste in the prepared mortars, represented by the binder-to-sand ratio. The ratio between cement and fine aggregate in regular cement mortars is usually 0.33 to 0.5. In that case, the

aggregate can impact the properties of the surface of the material, for example, its roughness. In the conducted study, the cement paste volume proved to be high enough compared to the volume of aggregate to mitigate its influence on surface properties completely.

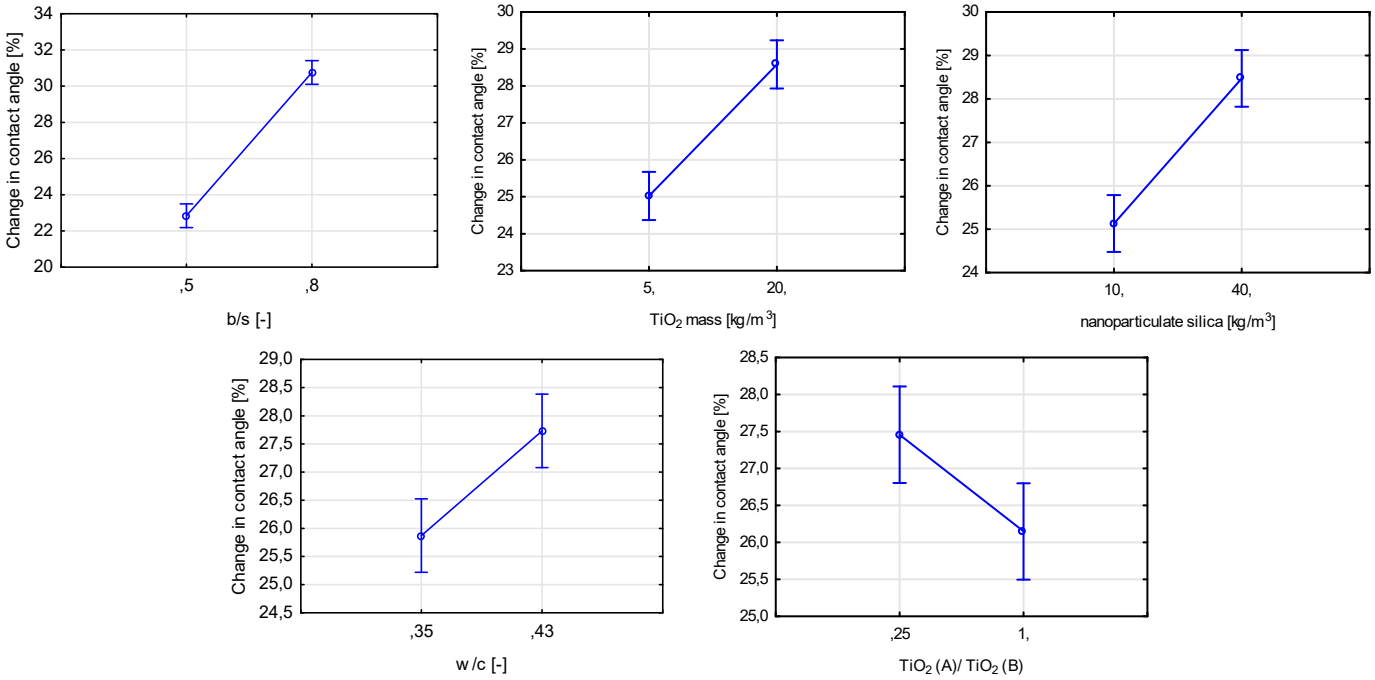

Figure 28. Marginal mean charts for statistically significant variables for self-cleaning via contact angle test in order of significance from the top left—b/s mass ratio, TiO_2 mass content, nanoparticulate silica content, w/c ratio, and the ratio between two types of titanium dioxide.

The lack of influence of the type of photocatalyst on the properties of photocatalytic mortars, despite the differences in their properties (mainly specific surface and crystallite size), was probably caused by the susceptibility of a TiO_2 of a higher specific surface area to agglomerate (TiO_2 (A)). Usually, the higher the surface area, the higher the risk of agglomeration of any material [36,37]. In the performed research, it is probable that TiO_2 (A), a photocatalyst of a higher potential in air purification, had reduced to a level comparable with TiO_2 (B). It could be argued that using photocatalysts of high specific surfaces could prove ineffective in cementitious composites; however, such a claim requires further studies on the subject.

5. Conclusions

Based on performed research, for the considered variables within the assumed scope of variability, several conclusions can be made:

- TiO_2 mass content and other components of cementitious materials have a statistically significant influence on both air purification from NO and NO_x and the self-cleaning properties of the material.
- Increasing the binder-to-sand ratio of the cementitious material instead of the mass content of titanium dioxide has a positive effect on the photocatalytic properties of the material.
- Nanoparticulate silica addition to the cementitious material has a negative effect on the air purification performance of the photocatalytic material.
- TiO_2 addition has a thickening effect on the rheological properties of cementitious materials and therefore limits the segregation of different components from the mix.
- Self-cleaning properties of photocatalytic materials, except for the mass content of titanium dioxide, depend on the binder-to-sand ratio and water-to-cement ratio.

- TiO_2 mass content does not influence the mechanical properties of photocatalytic mortars after seven days if added up to 20 kg/m^3.

Author Contributions: Conceptualization, M.K., K.C., W.J.-R. and B.R.; methodology, M.K., K.C., W.J.-R. and B.R.; software, M.K., K.C., W.J.-R. and B.R.; validation, W.J.-R.; formal analysis, W.J.-R.; investigation, M.K., K.C., W.J.-R. and B.R.; resources, W.J.-R.; data curation, M.K., K.C. and B.R.; writing—original draft preparation, M.K.; writing—review and editing, M.K., K.C., W.J.-R. and B.R.; visualization, M.K., K.C., W.J.-R. and B.R.; supervision, W.J.-R.; project administration, M.K., K.C., W.J.-R. and B.R.; funding acquisition, W.J.-R. All authors have read and agreed to the published version of the manuscript.

Funding: This research was funded by the NCBiR (National Centre for Research and Development), Poland under grant number TECHMATSTRATEG-III/0013/2019-01.

Institutional Review Board Statement: Not applicable.

Informed Consent Statement: Not applicable.

Data Availability Statement: Data is available on request.

Conflicts of Interest: The authors declare no conflict of interest.

References

1. Coelho, S.; Ferreira, J.; Rodrigues, V.; Lopes, M. Source apportionment of air pollution in European urban areas: Lessons from the ClairCity project. *J. Environ. Manag.* **2022**, *320*, 115899. [CrossRef]
2. Wu, L.; Mei, M.; Li, Z.; Liu, S.; Wang, X. Study on photocatalytic and mechanical properties of TiO2 modified pervious concrete. *Case Stud. Constr. Mater.* **2022**, *17*, e01606. [CrossRef]
3. Park, H.-J.; Hossain, S.M.; Choi, K.; Shon, H.-K.; Kim, J.-H. A Study on the Evaluation Methods of Nitrogen Oxide Removal Performance of Photocatalytic Concrete for Outdoor Applications. *Catalysts* **2022**, *12*, 846. [CrossRef]
4. McNaught, A.D.; Wilkinson, A. Compendium of Chemical Terminology, (The "Gold Book"), 2nd ed.Blackwell Scientific Publications: Oxford, UK. [CrossRef]
5. Witkowski, H.; Jackiewicz-Rek, W.; Jarosławski, J.; Chilmon, K.; Szkop, A. Ozone Formation during Photocatalytic Oxidation of Nitric Oxides under UV Irradiation with the Use of Commercial TiO_2 Photocatalytic Powders. *Materials* **2022**, *15*, 5905. [CrossRef] [PubMed]
6. Seinfeld, J.H.; Pandis, S.N. *Atmospheric Chemistry and Physics: From Air Pollution to Climate Change*, 3rd ed.; John Wiley & Sons: New Jersey, NJ, USA, 2016.
7. Russell, H.S.; Frederickson, L.B.; Hertel, O.; Ellermann, T.; Jensen, S.S. A Review of Photocatalytic Materials for Urban NOx Remediation. *Catalysts* **2021**, *11*, 675. [CrossRef]
8. Witkowski, H.; Jarosławski, J.; Tryfon-Bojarska, A. Application of Photocatalytic Concrete Paving Blocks in Poland—Verification of Effectiveness of Nitric Oxides Reduction and Novel Test Method. *Materials* **2020**, *13*, 5183. [CrossRef]
9. Goodeve, C.F.; Kitchener, J.A. Photosensitisation by titanium dioxide. *Trans. Faraday Soc.* **1938**, *34*, 570–579. [CrossRef]
10. Sokołowska, J.; Woyciechowski, P.; Kalinowski, M. Rheological Properties of Lunar Mortars. *Appl. Sci.* **2021**, *11*, 6961. [CrossRef]
11. Kalinowski, M.; Woyciechowski, P. Chloride Diffusion in Concrete Modified with Polyacrylic Superabsorbent Polymer (SAP) Hydrogel—The Influence of the Water-to-Cement Ratio and SAP-Entrained Water. *Materials* **2021**, *14*, 4064. [CrossRef]
12. Si, H.; Zhou, M.; Fang, Y.; He, J.; Yang, L.; Wang, F. Photocatalytic concrete for NOx degradation: Influence factors and durability. *Constr. Build. Mater.* **2021**, *298*, 123835. [CrossRef]
13. Herrmann, J.-M. Heterogeneous photocatalysis: Fundamentals and applications to the removal of various types of aqueous pollutants. *Catal. Today* **1999**, *53*, 115–129. [CrossRef]
14. Macphee, D.E.; Folli, A. Photocatalytic concretes—The interface between photocatalysis and cement chemistry. *Cem. Concr. Res.* **2016**, *85*, 48–54. [CrossRef]
15. Kvočka, D.; Šušteršič, J.; Mauko Pranjić, A.; Mladenović, A. Mass Concrete with EAF Steel Slag Aggregate: Workability, Strength, Temperature Rise, and Environmental Performance. *Sustainability* **2022**, *14*, 15502. [CrossRef]
16. Kępniak, M.; Woyciechowski, P.; Łukowski, P.; Kuziak, J.; Kobyłka, R. The Durability of Concrete Modified by Waste Limestone Powder in the Chemically Aggressive Environment. *Materials* **2019**, *12*, 1693. [CrossRef]
17. Bianchi, C.L.; Pirola, C.; Galli, F.; Cerrato, G.; Morandi, S.; Capucci, V. Pigmentary TiO2: A challenge for its use as photocatalyst in NOx air purification. *Chem. Eng. J.* **2015**, *261*, 76–82. [CrossRef]
18. Kumari, K.; Preetha, R.; Ramachandran, D.; Vishwakarma, V.; George, R.P.; Sundaramurthy, C.; Mudali, U.K.; Pillai, C.S. Nanoparticles for enhancing mechanical properties of fly ash concrete. *Mater. Today: Proc.* **2016**, *3*, 2387–2393. [CrossRef]
19. Liao, G.; Yao, W. Upcycling of waste concrete powder into a functionalized host for nano-TiO2 photocatalyst: Binding mechanism and enhanced photocatalytic efficiency. *J. Clean. Prod.* **2022**, *366*. [CrossRef]

20. *EN 197-1:2011*; Cement—Part 1: Composition, Specifications and Conformity Criteria for Common Cements. European Committee for Standardization: Brussels, Belgium, 2011.
21. *EN 13263-1:2005+A1:2009*; Silica Fume for Concrete-Part 1: Definitions, Requirements and Conformity Criteria. European Committee for Standardization: Brussels, Belgium, 2009.
22. *ISO 3262-13:1997*; Extenders—Specifications and Methods of Test—Part 13: Natural Quartz. International Organization for Standardization: Geneva, Switzerland, 1997.
23. *EN 13139:2002*; Aggregates for Mortar. European Committee for Standardization: Brussels, Belgium, 2002.
24. *EN 1008:2002*; Mixing water for concrete-Specification for sampling, testing and assessing the suitability of water, including water recovered from processes in the concrete industry, as mixing water for concrete. European Committee for Standardization: Brussels, Belgium, 2002.
25. *EN 934-2:2009+A1:2012*; Admixtures for concrete, mortar and grout-Part 2: Concrete admixtures-Definitions, requirements, conformity, marking and labelling. European Committee for Standardization: Brussels, Belgium, 2012.
26. *EN 196-1:2016*; Methods of testing cement-Part 1: Determination of strength. European Committee for Standardization: Brussels, Belgium, 2016.
27. *EN 1015-3:1999*; Methods of test for mortar for masonry-Part 3: Determination of consistence of fresh mortar (by flow table). European Committee for Standardization: Brussels, Belgium, 1999.
28. *ACI 237R-07*; Self-consolidating concrete. American Concrete Institute: Farmington Hills, MI, USA, 2019.
29. *BS ISO 27448:2009*; Test method for self-cleaning performance of semiconducting photocatalytic materials. Measurement of water contact angle. International Organization for Standardization: Geneva, Switzerland, 2009.
30. *UNI 11259:2016*; Photocatalysis-Determination of the photocatalytic activity of hydraulic binders-Rodammina test method. Ente Nazionale Italiano di Unificazione (UNI): Rome, Italy, 2016.
31. Rhee, I.; Lee, J.S.; Kim, J.B.; Kim, J.H. Nitrogen Oxides Mitigation Efficiency of Cementitious Materials Incorporated with TiO. *Materials* **2018**, *11*, 877. [CrossRef]
32. Zhou, Y.; Elchalakani, M.; Du, P.; Sun, C.; Zhang, Z.; Wang, H. Sunlight to heal mortar cracks: Photocatalytic self-healing mortar. *Cem. Concr. Compos.* **2023**, *135*, 104816. [CrossRef]
33. Senff, L.; Tobaldi, D.M.; Lemes-Rachadel, P.; Labrincha, J.A.; Hotza, D. The influence of TiO2 and ZnO powder mixtures on photocatalytic activity and rheological behavior of cement pastes. *Constr. Build. Mater.* **2014**, *65*, 191–200. [CrossRef]
34. Petrou, M.F.; Harries, K.A.; Gadala-Maria, F.; Kolli, V.G. A unique experimental method for monitoring aggregate settlement in concrete. *Cem. Concr. Res.* **2000**, *30*, 809–816. [CrossRef]
35. Ouyang, X.; Yu, L.; Wang, L.; Xu, S.; Ma, Y.; Fu, J. Surface properties of ceramic waste powder and its effect on the rheology, hydration and strength development of cement paste. *J. Build. Eng.* **2022**, *61*, 105253. [CrossRef]
36. Praveenkumar, T.R.; Vijayalakshmi, M.M.; Meddah, M.S. Strengths and durability performances of blended cement concrete with TiO_2 nanoparticles and rice husk ash. *Constr. Build. Mater.* **2019**, *217*, 343–351. [CrossRef]
37. Reches, Y.; Thomson, K.; Helbing, M.; Kosson, D.S.; Sanchez, F. Agglomeration and reactivity of nanoparticles of SiO_2, TiO2, Al_2O_3, Fe_2O_3, and clays in cement pastes and effects on compressive strength at ambient and elevated temperatures. *Constr. Build. Mater.* **2018**, *167*, 860–873. [CrossRef]